Article

Mass balance of the Greenland Ice Sheet from 1992 to 2018

https://doi.org/10.1038/s41586-019-1855-2

Received: 15 August 2019

Accepted: 25 November 2019

Published online: 10 December 2019

Check for updates

The IMBIE Team*

The Greenland Ice Sheet has been a major contributor to global sea-level rise in recent decades[1,2], and it is expected to continue to be so[3]. Although increases in glacier flow[4–6] and surface melting[7–9] have been driven by oceanic[10–12] and atmospheric[13,14] warming, the magnitude and trajectory of the ice sheet's mass imbalance remain uncertain. Here we compare and combine 26 individual satellite measurements of changes in the ice sheet's volume, flow and gravitational potential to produce a reconciled estimate of its mass balance. The ice sheet was close to a state of balance in the 1990s, but annual losses have risen since then, peaking at 345 ± 66 billion tonnes per year in 2011. In all, Greenland lost 3,902 ± 342 billion tonnes of ice between 1992 and 2018, causing the mean sea level to rise by 10.8 ± 0.9 millimetres. Using three regional climate models, we show that the reduced surface mass balance has driven 1,964 ± 565 billion tonnes (50.3 per cent) of the ice loss owing to increased meltwater runoff. The remaining 1,938 ± 541 billion tonnes (49.7 per cent) of ice loss was due to increased glacier dynamical imbalance, which rose from 46 ± 37 billion tonnes per year in the 1990s to 87 ± 25 billion tonnes per year since then. The total rate of ice loss slowed to 222 ± 30 billion tonnes per year between 2013 and 2017, on average, as atmospheric circulation favoured cooler conditions[15] and ocean temperatures fell at the terminus of Jakobshavn Isbræ[16]. Cumulative ice losses from Greenland as a whole have been close to the rates predicted by the Intergovernmental Panel on Climate Change for their high-end climate warming scenario[17], which forecast an additional 70 to 130 millimetres of global sea-level rise by 2100 compared with their central estimate.

The Greenland Ice Sheet holds enough water to raise mean global sea level by 7.4 m (ref. [18]). Its ice flows to the oceans through a network of glaciers and ice streams[19], each with a substantial inland catchment[20]. Fluctuations in the mass of the Greenland Ice Sheet occur due to variations in snow accumulation, meltwater runoff, ocean-driven melting and iceberg calving. There have been marked increases in air[21] and ocean[12] temperatures and reductions in summer cloud cover[22] around Greenland in the past few decades. These changes have produced increases in surface runoff[8], supraglacial lake formation[23] and drainage[24], iceberg calving[25], glacier terminus retreat[26], submarine melting[10,11] and ice flow[6], leading to widespread changes in the surface elevation—particularly near the margin of the ice sheet (Fig. 1).

Over recent decades, ice losses from Greenland have made a substantial contribution to global sea-level rise[2], and model projections suggest that this imbalance will continue in a warming climate[3]. Since the early 1990s there have been comprehensive satellite observations of changing ice sheet velocity[4,6], elevation[27–29] and, between 2002 and 2016, its changing gravitational attraction[30,31], from which complete estimates of Greenland Ice Sheet mass balance are determined[1]. Before the 1990s, only partial surveys of the ice sheet elevation[32] and velocity[33] change are available. In combination with models of surface mass balance (SMB; the net difference between precipitation, sublimation and meltwater runoff) and glacial isostatic adjustment[34], satellite measurements, reported by the 2012 Ice Sheet Mass Balance Intercomparison Exercise (IMBIE)[1], have shown a fivefold increase in the rate of ice loss from Greenland overall, rising from 51 ± 65 Gt yr^{-1} in the early 1990s to 263 ± 30 Gt yr^{-1} between 2005 and 2010. This ice loss has been driven by changes in SMB[7,21] and ice dynamics[5,33]. There was, however, a marked reduction in ice loss between 2013 and 2018, as a consequence of cooler atmospheric conditions and increased precipitation[15]. Although the broad pattern of change across Greenland (Fig. 1) is one of ice loss, there is considerable variability; for example, during the 2000s just four glaciers were responsible for half of the total ice loss due to increased discharge[5], whereas many others contribute today[33]. Moreover, some neighbouring ice streams have been observed to speed up over this period while others slowed down[35], suggesting diverse reasons for the changes that have taken place—including their geometrical configuration and basal conditions, as well as the forcing they have experienced[36]. In this study we combine satellite altimetry, gravimetry and ice velocity measurements to produce a reconciled estimate of the Greenland Ice Sheet mass balance between 1992 and 2018, we evaluate the impact of changes in SMB and uncertainty in glacial isostatic adjustment and we partition the ice sheet mass loss into signals associated with surface mass balance and ice dynamics. In doing so, we extend a previous assessment[1] to include more satellite and ancillary data and to cover the period since 2012.

*A list of participants and their affiliations appears at the end of the paper

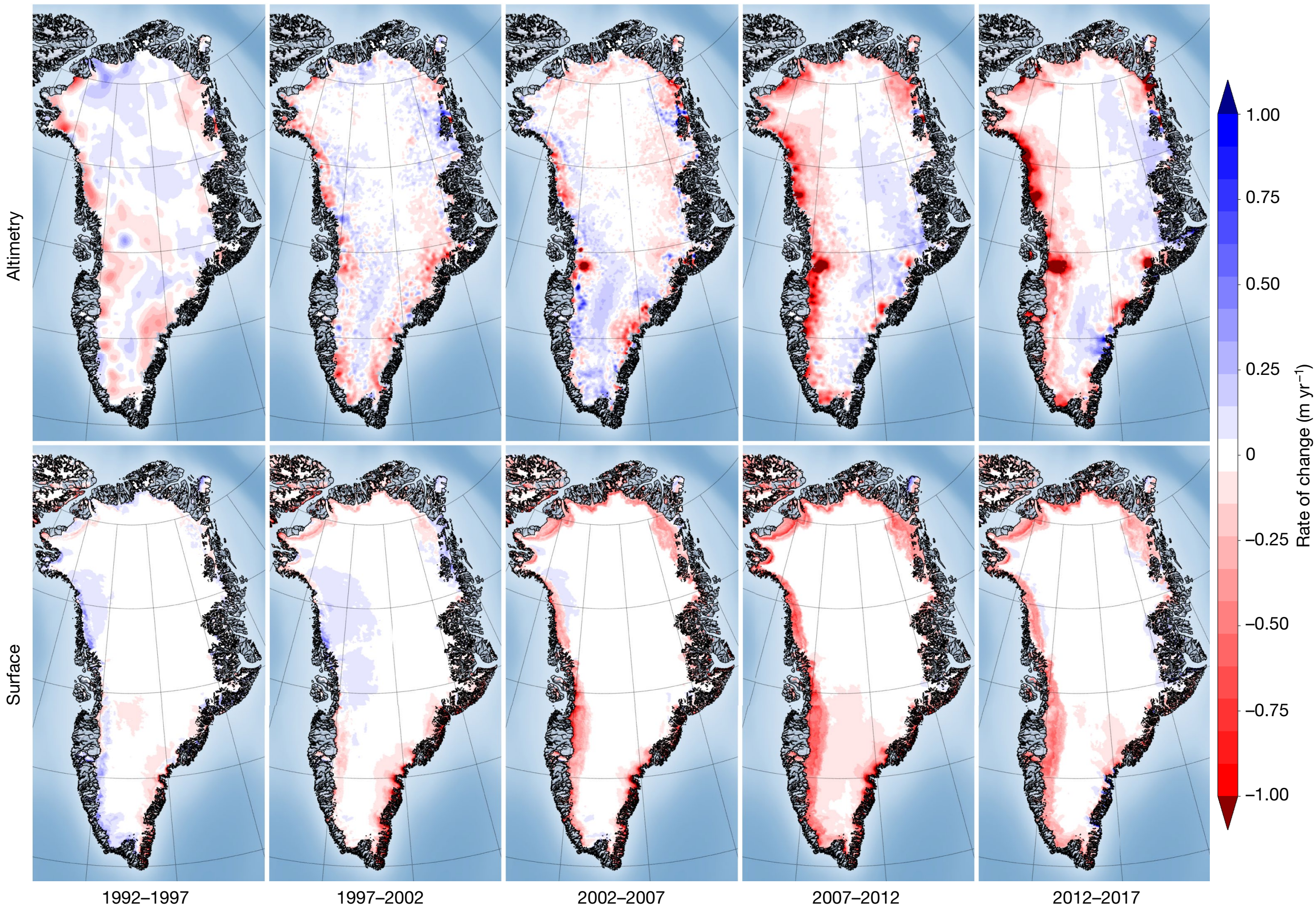

Fig. 1 | Greenland Ice Sheet elevation change. Rate of elevation change of the Greenland Ice Sheet determined from ERS, ENVISAT and CryoSat-2 satellite radar altimetry (top row) and from the HIRHAM5 SMB model (ice equivalent; bottom row) over successive 5-yr epochs. Data from ref. [29].

Data and methods

We use 26 estimates of ice sheet mass balance derived from satellite altimetry (9 datasets), satellite gravimetry (14 datasets) and the input–output method (3 datasets) to assess changes in the Greenland Ice Sheet mass balance. The satellite data were computed using common spatial[20,37] and temporal domains, and a range of models to estimate signals associated with changes in SMB and glacial isostatic adjustment. Satellite altimetry provides direct measurements of changing ice sheet surface elevation recorded at orbit crossing points[32], along repeated ground tracks[27] or using plane-fit solutions[28]. The ice sheet mass balance is estimated from these measurements either by prescribing the density of the elevation fluctuation[38] or by making an explicit model-based correction for changes in firn height[39]. Satellite gravimetry measures fluctuations in the Earth's gravitational field computed using either global spherical harmonic solutions[30] or using spatially discrete mass concentration units[31]. Ice sheet mass changes are determined after making model-based corrections for glacial isostatic adjustment[30]. The input–output method uses model estimates of SMB[7] (the input) and satellite observations of ice sheet velocity computed from radar[6] and optical[40] imagery combined with airborne measurements of ice thickness[33] to compute changes in marine-terminating glacier discharge into the oceans (the output). The overall mass balance is the difference between the input and output. Not all annual surveys of ice sheet discharge are complete, and sometimes regional extrapolations have to be employed to account for gaps in coverage[33]. Because they provide important ancillary data, we also assess six models of glacial isostatic adjustment and ten models of surface mass balance.

To compare and aggregate the individual satellite datasets, we first adopt a common approach to derive linear rates of ice sheet mass balance over 36-month intervals (see Methods). We then compute error-weighted averages of all altimetry, gravimetry and input–output group mass trends, and combine these into a single reconciled estimate of the ice sheet mass balance using error-weighting of the group trends. Uncertainties in the individual rates of mass change are estimated as the root sum square of the linear model misfit and their measurement error, uncertainties in the group rates are estimated as the root mean square of the contributing time-series errors and uncertainties in the reconciled rates are estimated as their root mean square error divided by the square root of the number of independent groups. Cumulative uncertainties are computed as the root sum square of annual errors, an approach that has been employed in numerous studies[1,17,33,41] and assumes that annual errors are not correlated over time. To improve on this assumption, it is necessary to consider the covariance of the systematic and random errors present in each mass balance solution (see Methods).

Intercomparison of satellite and model results

The satellite gravimetry and satellite altimetry data used in our assessment are corrected for the effects of glacial isostatic adjustment, although the correction is relatively small for altimetry as it manifests as a change in elevation and not mass. The most prominent and consistent local signals of glacial isostatic adjustment among the six models we considered are two instances of uplift peaking at about 5–6 mm yr^{-1}, one centred over northwest Greenland and Ellesmere Island, and one

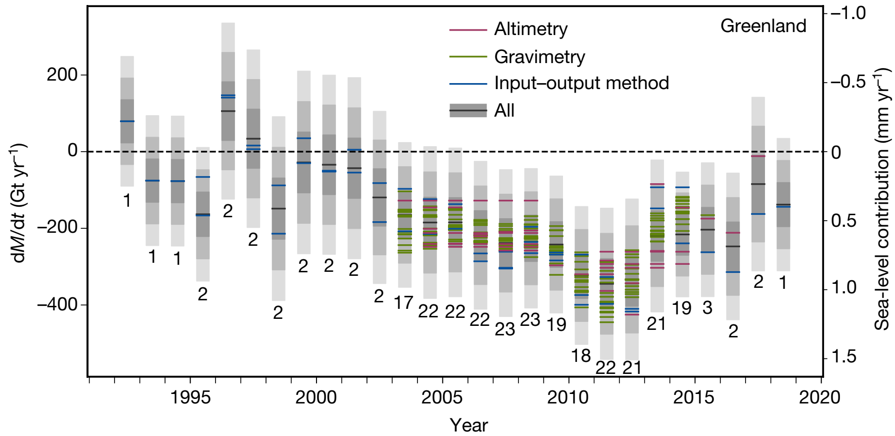

Fig. 2 | Greenland Ice Sheet mass balance. Rate of mass change (dM/dt, where M is mass and t time) of the Greenland Ice Sheet determined from the satellite-altimetry, input–output method and gravimetry assessments included in this study. In each case, dM/dt is computed at annual intervals from time series of relative mass change using a 3-yr window. An average of the estimates across each measurement technique is also shown for each year (black line). The estimated 1σ, 2σ and 3σ ranges of the class average are shaded in dark, mid and light grey, respectively; 97% of all estimates fall within the 1σ range, given their estimated individual errors. The equivalent sea-level contribution of the mass change is also indicated (right vertical axis), and the number of individual mass-balance estimates collated at each epoch is shown below each bar.

over northeast Greenland (see Methods and Extended Data Fig. 3). Although some models identify a 2 mm yr^{-1} subsidence under large parts of the central and southern parts of the ice sheet, it is absent or of lower magnitude in others, which suggests that it is less certain (Extended Data Table 1). The greatest difference among model solutions is at Kangerlussuaq Glacier in the southeast, where a study[42] has shown that models and observations agree if a localized weak Earth structure associated with overpassing the Iceland hotspot is assumed; the effect is to offset earlier estimates of mass trends associated with glacial isostatic adjustment by about 20 Gt yr^{-1}. Farther afield, the highest spread between modelled uplift occurs on Baffin Island and beyond due to variations in regional model predictions related to the demise of the Laurentide Ice Sheet[42]. This regional uncertainty is probably a major factor in the spread across the ice-sheet-wide estimates. Nevertheless, at −3 ± 20 Gt yr^{-1}, the mass signal associated with glacial isostatic adjustment in Greenland shows no coherent substantive change and is negligible relative to reported ice sheet mass trends[1].

There is generally good agreement between the models of Greenland Ice Sheet SMB that we have assessed for determining mass input—particularly those of a similar class; for example, 70% of all model estimates of runoff and accumulation fall within 1σ of their mean (see Methods and Extended Data Table 2). The exceptions are a global reanalysis with coarse spatial resolution that tends to underestimate runoff due to its poor delineation of the ablation zone, and a snow process model that tends to underestimate precipitation and to overestimate runoff in most sectors. Among the other eight models, the average surface mass balance between 1980 and 2012 is 361 ± 40 Gt yr^{-1}, with a marked negative trend over time (Extended Data Fig. 4) that is mainly due to increased runoff[7]. At the regional scale, the largest differences occur in the northeast, where two regional climate models predict considerably less runoff, and in the southeast, where there is considerable spread in precipitation and runoff across all models. All models show high temporal variability in SMB components, and all models show that the southeast receives the highest net intake of mass at the surface due to high rates of snowfall originating from the Icelandic Low[43]. By contrast, the southwest, which features the widest ablation zone[7], has experienced alternate periods of net surface mass loss and gain over recent decades, and has the lowest average SMB across the ice sheet.

We assessed the consistency of the satellite altimetry, gravimetry and input–output method estimates of Greenland Ice Sheet mass balance using common spatial and temporal domains (see Fig. 2 and Methods). In general, there is close agreement between estimates determined using each approach, and the standard deviations of annual mass balance solutions from the coincident altimetry, gravimetry and input–output methods are 42, 31 and 23 Gt yr^{-1}, respectively (Extended Data Table 3). Once averages were computed for each technique, the resulting estimates of mass balance were also closely aligned (Extended Data Fig. 6). For example, over the common period 2005–2015, the average Greenland Ice Sheet mass balance is −254 ± 18 Gt yr^{-1} and, by comparison, the spread of the altimetry, gravimetry and input–output method estimates is just 36 Gt yr^{-1} (Extended Data Table 3). The estimated uncertainty of the aggregated mass balance solution (see Methods) is larger than the standard deviation of model corrections for glacial isostatic adjustment (20 Gt yr^{-1} for gravimetry) and for surface mass balance (40 Gt yr^{-1}), which suggests that their collective impacts have been adequately compensated; it is also larger than the estimated 30 Gt yr^{-1} mass losses from peripheral ice caps[44], which are not accounted for in all individual solutions. In keeping with results from Antarctica[41], rates of mass loss determined using the input–output method are the most negative, and those determined from altimetry are the least negative. However, the spread among the three techniques is six times lower for Greenland than it is for Antarctica[41], reflecting differences in ice sheet size, the complexity of the mass balance processes and the limitations of the various geodetic techniques.

Ice sheet mass balance

We aggregated the average mass balance estimates from gravimetry, altimetry and the input–output method to form a single, time-varying record (Fig. 2) and then integrated these data to determine the cumulative mass lost from Greenland since 1992 (Fig. 3). Although Greenland has been losing ice throughout most of the intervening period, the rate of loss has varied considerably. The rate of ice loss progressively increased between 1992 and 2012, reaching a maximum of 345 ± 66 Gt yr^{-1} in 2011, ahead of the extreme summertime surface melting that occurred in the following year[14]. Since 2012, however, the trend has reversed, with a progressive reduction in the rate of mass loss during the subsequent period. By 2018—the last complete year of our survey—the annual rate of ice mass loss had reduced to 85 ± 75 Gt yr^{-1}. The highly variable nature of ice losses from Greenland is a consequence of the wide range of physical processes that are affecting different sectors of the ice sheet[16,28,35], which suggests that care should be taken when extrapolating measurements that

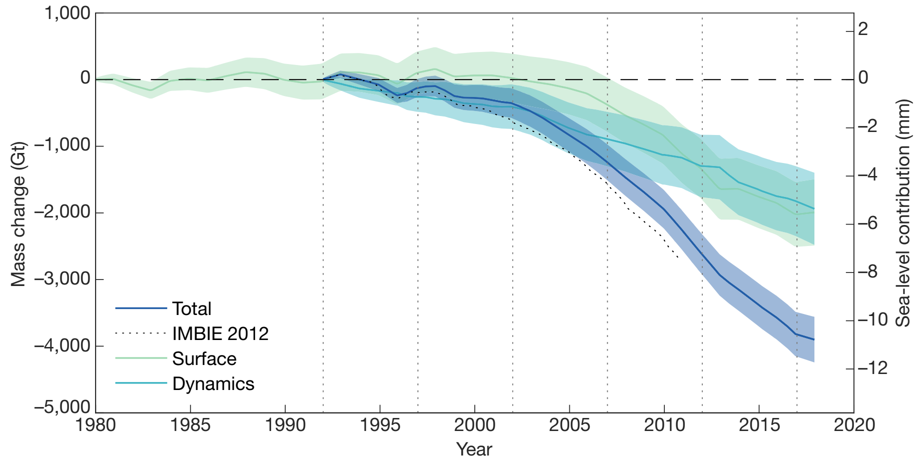

Fig. 3 | Cumulative anomalies in the total mass, SMB and ice dynamics of the Greenland Ice Sheet. The total change is determined as the integral of the average rate of ice sheet mass change (Fig. 2). The change in SMB is determined from three regional climate models relative to their mean over the period 1980–1990. The change associated with ice dynamics is determined as the difference between the change in total and surface mass. The estimated 1σ uncertainties of the cumulative changes are shown by the shaded envelopes. The dotted line shows the result of a previous assessment[1]. The equivalent sea-level contribution of the mass change is also indicated (right vertical axis). Vertical dashed lines mark consecutive 5-yr epochs since the start of our satellite record in 1992. The IMBIE 2012 data is from ref. [1].

are sparse in space or time. Although the rates of mass loss we have computed between 1992 and 2011 are 16% less negative than those of a previous assessment, which included far fewer datasets[1], the results are consistent given their respective uncertainties. Altogether, the Greenland Ice Sheet has lost 3,902 ± 342 Gt of ice to the ocean since 1992, with roughly half of this loss occurring during the 6-yr period between 2006 and 2012.

To determine the proportion of mass lost due to surface and ice dynamical processes, we computed the contemporaneous trend in Greenland Ice Sheet surface mass balance—the net balance between precipitation and ablation[7], which is controlled by interactions with the atmosphere (Fig. 3). In Greenland, recent trends in surface mass balance have been largely driven by meltwater runoff[43], which has increased as the regional climate has warmed[13]. As direct observations of ice sheet surface mass balance are too scarce to provide full temporal and spatial coverage[45], regional estimates are usually taken from atmospheric models that are evaluated with existing observations. Our evaluation (see Methods) shows that the finer-spatial-resolution regional climate models produce consistent results, probably due to their ability to capture local changes in melting and precipitation associated with atmospheric forcing, and to resolve the full extent of the ablation zone[46]. We therefore compare and combine estimates of Greenland SMB derived from three regional climate models: RACMO2.3p2[46], MARv3.6[21] and HIRHAM[9]. To assess the surface mass change across the Greenland Ice Sheet between 1980 and 2018, we accumulate SMB anomalies from each of the regional climate models (Extended Data Fig. 7) and average them into a single estimate (Fig. 3). These SMB anomalies are computed with respect to the average between 1980 and 1990, which corresponds to a period of approximate balance[8] and is common to all models. In this comparison, all three models show that the Greenland Ice Sheet entered abruptly into a period of anomalously low SMB in the late 1990s and, when combined, they show that the ice sheet lost 1,964 ± 565 Gt of its mass due to meteorological processes between 1992 and 2018 (Table 1).

Just over half (50.3%) of all mass losses from Greenland—and much of their short-term variability—have been due to variations in the ice sheet's SMB and its indirect impacts on firn processes. For example, between 2007 and 2012, 70% of the total ice loss (193 ± 37 Gt yr^{-1}) was due to SMB, compared with 27% (22 ± 20 Gt yr^{-1}) over the preceding 15 years and 57% (139 ± 38 Gt yr^{-1}) since then (Table 1). The rise in the total rate of ice loss during the late 2000s coincided with warmer atmospheric conditions, which promoted several episodes of widespread melting and runoff[14]. The reduction in surface mass loss since then is associated with a shift of the North Atlantic Oscillation, which brought about cooler atmospheric conditions and increased precipitation along the southeastern coast[15]. Trends in the total ice sheet mass balance are not entirely due to surface mass balance, however, and by calculating the difference between these two signals, we can estimate the total change in mass loss due to ice dynamical imbalance—that is, the integrated net mass loss from those glaciers whose velocity does not equal their long-term mean (Fig. 3). Although this approach is indirect, it makes use of all the satellite observations and regional climate models included in our study, overcoming limitations in the spatial and temporal sampling of ice discharge estimates derived from ice velocity and thickness data. Our estimate shows that, between 1992 and 2018, Greenland lost 1,938 ± 541 Gt of ice due to the dynamical imbalance of glaciers relative to their steady state, accounting for 49.7% of the total imbalance (Table 1). Losses due to increased ice discharge rose

Table 1 | Rates of Greenland Ice Sheet total, surface and dynamical mass change

Region	1992–1997 (Gt yr^{-1})	1997–2002 (Gt yr^{-1})	2002–2007 (Gt yr^{-1})	2007–2012 (Gt yr^{-1})	2012–2017 (Gt yr^{-1})	1992–2011 (Gt yr^{-1})	1992–2018 (Gt yr^{-1})
Total	−26 ± 27	−44 ± 35	−174 ± 30	−275 ± 28	−244 ± 28	−119 ± 16	−150 ± 13
Surface	26 ± 35	−15 ± 36	−78 ± 36	−193 ± 37	−139 ± 38	−57 ± 18	−76 ± 16
Dynamics	−52 ± 44	−29 ± 50	−96 ± 47	−82 ± 46	−105 ± 47	−62 ± 24	−75 ± 21

Total rates were determined from all satellite measurements over the various epochs, rates of surface mass change were determined from three regional climate models and rates of dynamical mass change were determined as the difference between the two. The period 1992–2011 is included for comparison with a previous assessment[1], which reported a mass balance estimate of −142 ± 49 Gt yr^{-1} based on far fewer data. The small differences in our updated estimate are due to our inclusion of more data and an updated aggregation scheme (see Methods). Errors are 1σ.

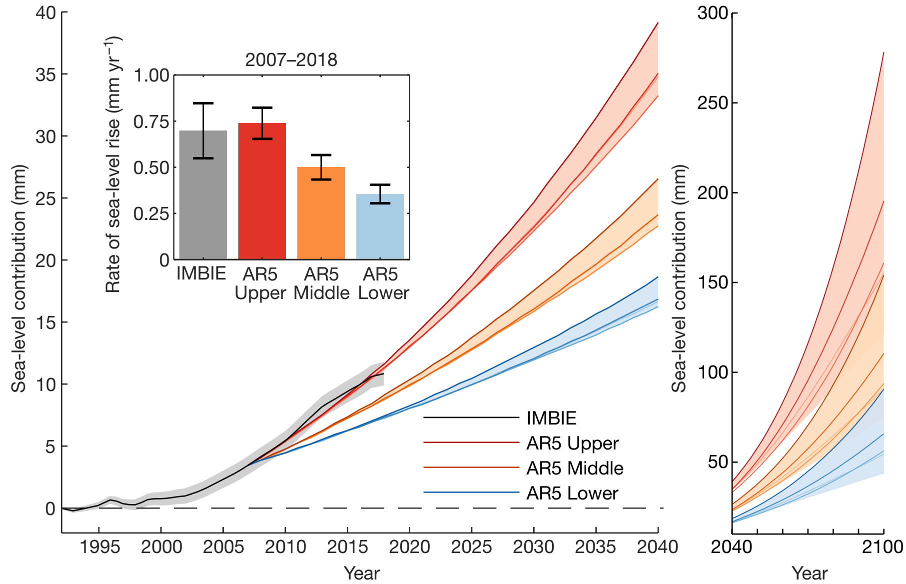

Fig. 4 | Observed and predicted sea-level contributions from Greenland Ice Sheet mass change. The global sea-level contribution from Greenland Ice Sheet mass change according to this study and the IPCC AR5 projections between 1992–2040 (left) and 2040–2100 (right) including upper, mid and lower estimates from the sum of modelled SMB and rapid ice dynamical contributions. Darker lines represent pathways from the five AR5 scenarios in order of increasing emissions: RCP2.6, RCP4.5, RCP6.0, SRES A1B and RCP8.5. Shaded areas represent the spread of AR5 emissions scenarios and the 1σ estimated error on the IMBIE data (this study). Inset, the average annual rates of sea-level rise during the overlap period 2007–2018 and their standard deviations (error bars). Cumulative AR5 projections have been offset to make them equal to the observational record at their start date (2007).

sharply in the early 2000s when Jakobshavn Isbræ[10] and several other outlet glaciers in the southeast[47] sped up, and the discharge losses are now four times higher than in the 1990s. For the period between 2002 and 2007, ice dynamical imbalance was the major source of ice loss from the ice sheet as a whole, although the situation has since returned to being dominated by surface mass losses as several glaciers have slowed down[16].

Despite a reduction in the overall rate of ice loss from Greenland between 2013 and 2018 (Fig. 2), the ice sheet mass balance remained negative, adding 10.8 ± 0.9 mm to global sea level since 1992. Although the average sea level contribution is 0.42 ± 0.04 mm yr^{-1}, the 5-yr average rate varied by a factor of 5 over the 25-yr period, peaking at 0.76 ± 0.08 mm yr^{-1} between 2007 and 2012. The variability in ice loss from Greenland illustrates the importance of accounting for annual fluctuations when attempting to close the global sea-level budget[2]. Satellite records of ice sheet mass balance are also an important tool for evaluating numerical models of ice sheet evolution[48]. In their 2013 assessment, the Intergovernmental Panel on Climate Change (IPCC) predicted ice losses from Greenland due to SMB and glacier dynamics under a range of scenarios, beginning in 2007[17] (Fig. 4). Although ice losses from Greenland have fluctuated considerably during the 12-yr period of overlap between the IPCC predictions and our reconciled time series, the total change and average rate (0.70 mm yr^{-1}) are close to the upper range of predictions (0.72 mm yr^{-}), which implies 70–130 mm of sea-level rise by 2100 above central estimates. The drop in ice losses between 2013 and 2018, however, shifted rates towards the lower end of projections, and a longer period of comparison is required to establish whether the upper trajectory will continue to be followed. Even greater sea-level contributions cannot be ruled out if feedbacks between the ice sheet and other elements of the climate system are underestimated by current ice sheet models[3]. Although the volume of ice stored in Greenland is a small fraction of that in Antarctica (12%), its recent losses have been ~38% higher[41] as a consequence of the relatively strong atmospheric[13,14] and oceanic[10,11] warming that has occurred in its vicinity, and it is expected to continue to be a major source of sea-level rise[3,17].

Conclusions

We combine 26 satellite estimates of ice sheet mass balance and assess 10 models of ice sheet SMB and 6 models of glacial isostatic adjustment to show that the Greenland Ice Sheet lost 3,902 ± 342 Gt of ice between 1992 and 2018. During the common period 2005–2015, the spread of mass balance estimates derived from three techniques is 36 Gt yr^{-1}, or 14% of the estimated rate of imbalance. The rate of ice loss has generally increased over time, rising from 26 ± 27 Gt yr^{-1} between 1992 and 1997, peaking at 275 ± 28 Gt yr^{-1} between 2007 and 2012, and reducing to 244 ± 28 Gt yr^{-1} between 2012 and 2017. Just over half (1,964 ± 565 Gt, or 50.3%) of the ice losses are due to reduced SMB (mostly meltwater runoff) associated with changing atmospheric conditions[13,14], and these changes have also driven the shorter-term temporal variability in ice sheet mass balance. Despite variations in the imbalance of individual glaciers[4,5,33], ice losses due to increasing discharge from the ice sheet as a whole have risen steadily from 46 ± 37 Gt yr^{-1} in the 1990s to 87 ± 25 Gt yr^{-1} since then, and account for just under half of all losses (49.7%) over the survey period.

Our assessment shows that estimates of Greenland Ice Sheet mass balance derived from satellite altimetry, gravimetry and the input–output method agree to within 20 Gt yr^{-1}, that model estimates of SMB agree to within 40 Gt yr^{-1} and that model estimates of glacial isostatic adjustment agree to within 20 Gt yr^{-1}. These differences represent a small fraction (13%) of the Greenland Ice Sheet mass imbalance and are comparable to its estimated uncertainty (13 Gt yr^{-1}). Nevertheless, there is still disagreement among models of glacial isostatic adjustment in northern Greenland. Spatial resolution is a key factor in the degree to which models of SMB can represent ablation and precipitation at local scales, and estimates of ice sheet mass balance determined from satellite altimetry and the input–output method continue to be positively and negatively biased, respectively, compared with those based on satellite gravimetry (albeit by small amounts). More satellite estimates of ice sheet mass balance at the start (1990s) and end (2010s) of our record would help to reduce the dependence on fewer data during those periods; although new missions[49,50] will no doubt address the latter period, further analysis of historical satellite data are required to address the paucity of data during the early years.

Online content

Any methods, additional references, Nature Research reporting summaries, source data, extended data, supplementary information, acknowledgements, peer review information; details of author contributions and competing interests; and statements of data and code availability are available at https://doi.org/10.1038/s41586-019-1855-2.

1. Shepherd, A. et al. A reconciled estimate of ice-sheet mass balance. *Science* **338**, 1183–1189 (2012).
2. WCRP Global Sea Level Budget Group. Global sea-level budget 1993–present. *Earth Syst. Sci. Data* **10**, 1551–1590 (2018).
3. Pattyn, F. et al. The Greenland and Antarctic ice sheets under 1.5 °C global warming. *Nat. Clim. Change* **8**, 1053–1061 (2018).
4. Moon, T., Joughin, I., Smith, B. & Howat, I. 21st-century evolution of Greenland outlet glacier velocities. *Science* **336**, 576–578 (2012).
5. Enderlin, E. M. et al. An improved mass budget for the Greenland ice sheet. *Geophys. Res. Lett*. **41**, 866–872 (2014).
6. Rignot, E. & Kanagaratnam, P. Changes in the velocity structure of the Greenland Ice Sheet. *Science* **311**, 986–990 (2006).
7. van den Broeke, M. et al. Partitioning recent Greenland mass loss. *Science* **326**, 984–986 (2009).
8. Trusel, L. D. et al. Nonlinear rise in Greenland runoff in response to post-industrial Arctic warming. *Nature* **564**, 104–108 (2018).
9. Lucas-Picher, P. et al. Very high resolution regional climate model simulations over Greenland: identifying added value. *J. Geophys. Res. D* **117**, 02108 (2012).
10. Holland, D. M., Thomas, R. H., de Young, B., Ribergaard, M. H. & Lyberth, B. Acceleration of Jakobshavn Isbræ triggered by warm subsurface ocean waters. *Nat. Geosci*. **1**, 659–664 (2008).
11. Seale, A., Christoffersen, P., Mugford, R. I. & O'Leary, M. Ocean forcing of the Greenland Ice Sheet: calving fronts and patterns of retreat identified by automatic satellite monitoring of eastern outlet glaciers. *J. Geophys. Res. Earth Surf*. **116**, F03013 (2011).
12. Straneo, F. & Heimbach, P. North Atlantic warming and the retreat of Greenland's outlet glaciers. *Nature* **504**, 36–43 (2013).
13. Hanna, E., Mernild, S. H., Cappelen, J. & Steffen, K. Recent warming in Greenland in a long-term instrumental (1881–2012) climatic context: I. Evaluation of surface air temperature records. *Environ. Res. Lett*. **7**, 045404 (2012).
14. Fettweis, X. et al. Important role of the mid-tropospheric atmospheric circulation in the recent surface melt increase over the Greenland ice sheet. *Cryosphere* **7**, 241–248 (2013).
15. Bevis, M. et al. Accelerating changes in ice mass within Greenland, and the ice sheet's sensitivity to atmospheric forcing. *Proc. Natl Acad. Sci. USA* **116**, 1934–1939 (2019).
16. Khazendar, A. et al. Interruption of two decades of Jakobshavn Isbrae acceleration and thinning as regional ocean cools. *Nat. Geosci*. **12**, 277–283 (2019); correction **12**, 493 (2019).
17. Church, J. A. et al. in *Climate Change 2013: The Physical Science Basis* (eds Stocker, T. F. et al.) 1137–1216 (IPCC, Cambridge Univ. Press, 2013).
18. Morlighem, M. et al. BedMachine v3: complete bed topography and ocean bathymetry mapping of Greenland from multibeam echo sounding combined with mass conservation. *Geophys. Res. Lett*. **44**, 11,051–11,061 (2017).
19. Joughin, I., Smith, B. E., Howat, I. M., Scambos, T. & Moon, T. Greenland flow variability from ice-sheet-wide velocity mapping. *J. Glaciol*. **56**, 415–430 (2010).
20. Zwally, H. J., Giovinetto, M. B., Beckley, M. A. & Saba, J. L. *Antarctic and Greenland Drainage Systems* (GSFC Cryospheric Sciences Laboratory, 2012); http://icesat4.gsfc.nasa.gov/cryo_data/ant_grn_drainage_systems.php.
21. Fettweis, X. et al. Reconstructions of the 1900–2015 Greenland ice sheet surface mass balance using the regional climate MAR model. *Cryosphere* **11**, 1015–1033 (2017).
22. Hofer, S., Tedstone, A. J., Fettweis, X. & Bamber, J. L. Decreasing cloud cover drives the recent mass loss on the Greenland Ice Sheet. *Sci. Adv*. **3**, e1700584 (2017).
23. Leeson, A. A. et al. Supraglacial lakes on the Greenland ice sheet advance inland under warming climate. *Nat. Clim. Change* **5**, 51–55 (2015).
24. Palmer, S., McMillan, M. & Morlighem, M. Subglacial lake drainage detected beneath the Greenland ice sheet. *Nat. Commun*. **6**, 8408 (2015).
25. Nick, F. M. et al. The response of Petermann Glacier, Greenland, to large calving events, and its future stability in the context of atmospheric and oceanic warming. *J. Glaciol*. **58**, 229–239 (2012).
26. Joughin, I. et al. Ice-front variation and tidewater behavior on Helheim and Kangerdlugssuaq Glaciers, Greenland. *J. Geophys. Res. Earth Surf*. **113**, F01004 (2008).
27. Pritchard, H. D., Arthern, R. J., Vaughan, D. G. & Edwards, L. A. Extensive dynamic thinning on the margins of the Greenland and Antarctic ice sheets. *Nature* **461**, 971–975 (2009).
28. McMillan, M. et al. A high-resolution record of Greenland mass balance. *Geophys. Res. Lett*. **43**, 7002–7010 (2016).
29. Sandberg Sørensen, L. et al. 25 years of elevation changes of the Greenland Ice Sheet from ERS, Envisat, and CryoSat-2 radar altimetry. *Earth Planet. Sci. Lett*. **495**, 234–241 (2018).
30. Velicogna, I. & Wahr, J. Greenland mass balance from GRACE. *Geophys. Res. Lett*. **32**, L18505 (2005).
31. Luthcke, S. B. et al. Recent Greenland ice mass loss by drainage system from satellite gravity observations. *Science* **314**, 1286–1289 (2006).
32. Zwally, H. J., Bindschadler, R. A., Brenner, A. C., Major, J. A. & Marsh, J. G. Growth of Greenland Ice Sheet: measurement. *Science* **246**, 1587–1589 (1989).
33. Mouginot, J. et al. Forty-six years of Greenland Ice Sheet mass balance from 1972 to 2018. *Proc. Natl Acad. Sci. USA* **116**, 9239–9244 (2019).
34. Lecavalier, B. S. et al. A model of Greenland ice sheet deglaciation constrained by observations of relative sea level and ice extent. *Quat. Sci. Rev*. **102**, 54–84 (2014).
35. King, M. D. et al. Seasonal to decadal variability in ice discharge from the Greenland Ice Sheet. *Cryosphere* **12**, 3813–3825 (2018).
36. Porter, D. F. et al. Identifying spatial variability in Greenland's outlet glacier response to ocean heat. *Front. Earth Sci*. **6**, 90 (2018).
37. Rignot, E. & Mouginot, J. Ice flow in Greenland for the International Polar Year 2008–2009. *Geophys. Res. Lett*. **39**, L11501 (2012).
38. Sørensen, L. S. et al. Mass balance of the Greenland ice sheet (2003–2008) from ICESat data—the impact of interpolation, sampling and firn density. *Cryosphere* **5**, 173–186 (2011).
39. Zwally, H. J. et al. Greenland ice sheet mass balance: distribution of increased mass loss with climate warming; 2003–07 versus 1992–2002. *J. Glaciol*. **57**, 88–102 (2011).
40. Rosenau, R., Scheinert, M. & Dietrich, R. A processing system to monitor Greenland outlet glacier velocity variations at decadal and seasonal time scales utilizing the Landsat imagery. *Remote Sens. Environ*. **169**, 1–19 (2015).
41. The IMBIE Team. Mass balance of the Antarctic Ice Sheet from 1992 to 2017. *Nature* **558**, 219–222 (2018).
42. Khan, S. A. et al. Geodetic measurements reveal similarities between post–Last Glacial Maximum and present-day mass loss from the Greenland ice sheet. *Sci. Adv*. **2**, e1600931 (2016).
43. Ettema, J. et al. Higher surface mass balance of the Greenland ice sheet revealed by high-resolution climate modeling. *Geophys. Res. Lett*. **36**, L12501 (2009).
44. Bolch, T. et al. Mass loss of Greenland's glaciers and ice caps 2003–2008 revealed from ICESat laser altimetry data. *Geophys. Res. Lett*. **40**, 875–881 (2013).
45. Vernon, C. L. et al. Surface mass balance model intercomparison for the Greenland ice sheet. *Cryosphere* **7**, 599–614 (2013).
46. Noël, B. et al. Modelling the climate and surface mass balance of polar ice sheets using RACMO2—Part 1: Greenland (1958–2016). *Cryosphere* **12**, 811–831 (2018).
47. Howat, I. M., Joughin, I., Fahnestock, M., Smith, B. E. & Scambos, T. A. Synchronous retreat and acceleration of southeast Greenland outlet glaciers 2000–06: ice dynamics and coupling to climate. *J. Glaciol*. **54**, 646–660 (2008).
48. Shepherd, A. & Nowicki, S. Improvements in ice-sheet sea-level projections. *Nat. Clim. Change* **7**, 672–674 (2017).
49. Markus, T. et al. The Ice, Cloud, and land Elevation Satellite-2 (ICESat-2): science requirements, concept, and implementation. *Remote Sens. Environ*. **190**, 260–273 (2017).
50. Flechtner, F. et al. What can be expected from the GRACE-FO laser ranging interferometer for earth science applications? *Surv. Geophys*. **37**, 453–470 (2016).

Publisher's note Springer Nature remains neutral with regard to jurisdictional claims in published maps and institutional affiliations.

The IMBIE Team

Andrew Shepherd[1]✉, Erik Ivins[2], Eric Rignot[2,3], Ben Smith[4], Michiel van den Broeke[5], Isabella Velicogna[2,3], Pippa Whitehouse[6], Kate Briggs[1], Ian Joughin[4], Gerhard Krinner[7], Sophie Nowicki[8], Tony Payne[9], Ted Scambos[10], Nicole Schlegel[2], Geruo A[3], Cécile Agosta[11], Andreas Ahlstrøm[12], Greg Babonis[13], Valentina R. Barletta[14], Anders A. Bjørk[15], Alejandro Blazquez[16], Jennifer Bonin[17], William Colgan[12], Beata Csatho[13], Richard Cullather[18], Marcus E. Engdahl[19], Denis Felikson[8], Xavier Fettweis[11], Rene Forsberg[14], Anna E. Hogg[1], Hubert Gallee[7], Alex Gardner[2], Lin Gilbert[20], Noel Gourmelen[21], Andreas Groh[22], Brian Gunter[23], Edward Hanna[24], Christopher Harig[25], Veit Helm[26], Alexander Horvath[27], Martin Horwath[22], Shfaqat Khan[14], Kristian K. Kjeldsen[12,28], Hannes Konrad[29], Peter L. Langen[30], Benoit Lecavalier[31], Bryant Loomis[8], Scott Luthcke[8], Malcolm McMillan[32], Daniele Melini[33], Sebastian Mernild[34,35,36,37], Yara Mohajerani[3], Philip Moore[38], Ruth Mottram[30], Jeremie Mouginot[3,7], Gorka Moyano[39], Alan Muir[20], Thomas Nagler[40], Grace Nield[6], Johan Nilsson[2], Brice Noël[5], Ines Otosaka[1], Mark E. Pattle[39], W. Richard Peltier[41], Nadège Pie[42], Roelof Rietbroek[43], Helmut Rott[40], Louise Sandberg Sørensen[14], Ingo Sasgen[26], Himanshu Save[42], Bernd Scheuchl[3], Ernst Schrama[44], Ludwig Schröder[22,26], Ki-Weon Seo[45], Sebastian B. Simonsen[14], Thomas Slater[1], Giorgio Spada[46], Tyler Sutterley[3], Matthieu Talpe[2], Lev Tarasov[31], Willem Jan van de Berg[5], Wouter van der Wal[44,47], Melchior van Wessem[5], Bramha Dutt Vishwakarma[48], David Wiese[2], David Wilton[49], Thomas Wagner[50], Bert Wouters[5,47] & Jan Wuite[40]

[1]Centre for Polar Observation and Modelling, University of Leeds, Leeds, UK. [2]NASA Jet Propulsion Laboratory, California Institute of Technology, Pasadena, CA, USA. [3]Department of Earth System Science, University of California, Irvine, CA, USA. [4]Department of Earth and Space Sciences, University of Washington, Seattle, WA, USA. [5]Institute for Marine and Atmospheric Research, Utrecht University, Utrecht, The Netherlands. [6]Department of Geography, Durham University, Durham, UK. [7]Institute of Environmental Geosciences, Université Grenoble Alpes, Grenoble, France. [8]Cryospheric Sciences Laboratory, NASA Goddard Space Flight Center, Greenbelt, MD, USA. [9]School of Geographical Sciences, University of Bristol, Bristol, UK. [10]Earth Science and Observation Center, University of Colorado, Boulder, CO, USA. [11]Department of Geography, University of Liège, Liège, Belgium. [12]Geological Survey of Denmark and Greenland, Copenhagen, Denmark. [13]Department of Geology, State University of New York at Buffalo, Buffalo, NY, USA. [14]DTU Space, National Space Institute, Technical University of Denmark, Kongens Lyngby, Denmark. [15]Department of Geosciences and Natural Resource Management, University of Copenhagen, Copenhagen, Denmark. [16]LEGOS, Université de Toulouse, Toulouse, France. [17]College of

Marine Sciences, University of South Florida, Tampa, FL, USA. [18]Global Modeling and Assimilation Office, NASA Goddard Space Flight Center, Greenbelt, MD, USA. [19]ESA-ESRIN, Frascati, Italy. [20]Mullard Space Science Laboratory, University College London, Holmbury St Mary, UK. [21]School of Geosciences, University of Edinburgh, Edinburgh, UK. [22]Institute for Planetary Geodesy, Technische Universität Dresden, Dresden, Germany. [23]Daniel Guggenheim School of Aerospace Engineering, Georgia Institute of Technology, Atlanta, GA, USA. [24]School of Geography, University of Lincoln, Lincoln, UK. [25]Department of Geosciences, University of Arizona, Tucson, AZ, USA. [26]Alfred Wegener Institute, Helmholtz Centre for Polar and Marine Research, Bremerhaven, Germany. [27]Institute of Astronomical and Physical Geodesy, Technical University Munich, Munich, Germany. [28]GeoGenetics, Globe Institute, University of Copenhagen, Copenhagen, Denmark. [29]Deutscher Wetterdienst, Offenbach, Germany. [30]Danish Meteorological Institute, Copenhagen, Denmark. [31]Department of Physics and Physical Oceanography, Memorial University of Newfoundland, St. John's, Newfoundland and Labrador, Canada. [32]Lancaster Environment Centre, University of Lancaster, Lancaster, UK. [33]Istituto Nazionale di Geofisica e Vulcanologia, Rome, Italy. [34]Nansen Environmental and Remote Sensing Centre, Bergen, Norway. [35]Faculty of Engineering and Science, Western Norway University of Applied Sciences, Sogndal, Norway. [36]Direction of Antarctic and Sub-Antarctic Programs, Universidad de Magallanes, Punta Arenas, Chile. [37]Geophysical Institute, University of Bergen, Bergen, Norway. [38]School of Engineering, Newcastle University, Newcastle upon Tyne, UK. [39]isardSAT, Barcelona, Catalonia. [40]ENVEO, Innsbruck, Austria. [41]Department of Physics, University of Toronto, Toronto, Ontario, Canada. [42]Center for Space Research, University of Texas, Austin, TX, USA. [43]Institute of Geodesy and Geoinformation, University of Bonn, Bonn, Germany. [44]Department of Space Engineering, Delft University of Technology, Delft, The Netherlands. [45]Department of Earth Science Education, Seoul National University, Seoul, South Korea. [46]Dipartimento di Scienze Pure e Applicate, Università di Urbino "Carlo Bo", Urbino, Italy. [47]Department of Civil Engineering, Delft University of Technology, Delft, The Netherlands. [48]Geodetic Institute, University of Stuttgart, Stuttgart, Germany. [49]Department of Computer Science, University of Sheffield, Sheffield, UK. [50]NASA Headquarters, Washington, DC, USA. ✉e-mail: a.shepherd@leeds.ac.uk

Methods

Data

In this assessment, we analyse five groups of data: estimates of ice sheet mass-balance determined from three distinct classes of satellite observations (altimetry, gravimetry and the input–output method (IOM)) and model estimates of SMB) and glacial isostatic adjustment (GIA). Each dataset is computed following previously reported methods (based on refs. [28,33,38,51–119] and detailed in Supplementary Table 1) and, for consistency, they are aggregated within common spatial and temporal domains. Altogether, 26 separate ice sheet mass balance datasets were used—9 derived from satellite altimetry, 3 from the IOM and 14 from satellite gravimetry—with a combined period running from 1992 to 2018 (Extended Data Fig. 1). We also assess six model estimates of GIA (Extended Data Table 1) and ten model estimates of SMB (Extended Data Table 2).

Drainage basins

We analyse mass trends using two ice sheet drainage basin sets (Extended Data Fig. 2) for consistency with those used in the first IMBIE assessment[1] and to evaluate an updated definition tailored towards mass budget assessments. The first set comprises 19 drainage basins delineated using surface elevation maps derived from ICESat-1 with a total area of 1,703,625 km^2 (ref. [20]). The second drainage basin set is an updated definition that considers other factors such as the direction of ice flow and includes 6 basins with a combined area of 1,723,300 km^2 (ref. [37]). The two drainage basin sets differ by 1% in area at the scale of the Greenland Ice Sheet, and this has a negligible impact on mass trends when compared to the estimated uncertainty of individual techniques.

Glacial isostatic adjustment

GIA (the delayed response of Earth's interior to temporal changes in ice loading) affects estimates of ice sheet mass balance determined from satellite gravimetry and, to a lesser extent, satellite altimetry[93]. Here, we compare six independent models of GIA in the vicinity of the Greenland Ice Sheet (Extended Data Table 1). The GIA model solutions we considered differ for a variety of reasons, including differences in their physics, in their computational approach, in their prescriptions of solid Earth unloading during the last glacial cycle and their Earth rheology, and in the datasets against which they are evaluated. Although alternative ice histories (for example, ref. [94]) and mantle viscosities (for example, ref. [95]) are available, we restricted our comparison to those that contributed to our assessment. No approach is generally accepted as optimal, and so we evaluate the models by computing the mean and standard deviation of their predicted uplift rates (Extended Data Fig. 3). We also estimate the contribution of each model to gravimetric mass trends using a common processing approach[41] that puts special emphasis on the treatment of low spherical harmonic degrees in the GIA-related trends in the gravitational field.

The highest rates of GIA-related uplift occur in northern Greenland, although this region also exhibits marked variability among the solutions, as does the area around Kangerlussuaq Glacier to the southeast. Even though the model spread is high in northern Greenland, the signal in this sector is also consistently high in most solutions. However, none of the GIA models considered here fully captures all areas of high uplift present in the models, and so it is possible there is a bias towards low values in the average field across the ice sheet overall. The models yield an average adjustment for GRACE estimates of the Greenland Ice Sheet mass balance of −3 Gt yr^{-1}, with a standard deviation of around 20 Gt yr^{-1}. The spread is probably due, in part, to differences in the way each model accounts for GIA in North America (which is ongoing and impacts western Greenland), and so care must be taken when estimating mass balance at the basin scale. Local misrepresentation of the solid Earth response can also have a relatively large impact stemming especially from lateral variations of solid Earth properties[42,51], and revisions of the current state of knowledge can be expected[34].

SMB

Here, ice-sheet SMB is defined as total precipitation minus sublimation, evaporation and meltwater runoff; that is, the interaction of the atmosphere and the superficial snow and firn layers, for example through mass exchanges via precipitation, sublimation and runoff, and through mass redistribution by snowdrift, melting and refreezing. We compare ten estimates of Greenland Ice Sheet SMB derived using a range of alternative approaches; four regional climate models (RCMs), two downscaled RCMs, a global reanalysis, two downscaled model reanalyses of climate data and one gridded model of snow processes driven by climate model output (Extended Data Table 2).

Although SMB models of similar classes tend to produce similar results, there are larger differences between classes—most notably the global reanalysis and the process model—which lead to estimates of SMB that are substantially higher and lower than all other solutions, respectively. The regional climate model solutions agree well at the scale of individual drainage sectors, with the largest differences occurring in northeast Greenland (Extended Data Fig. 4). The snow process model tends to underestimate SMB when compared with the other solutions that we have considered in various sectors of the ice sheet, at times even yielding negative SMB, while the global reanalysis tends to overestimate it.

Across all models, the average SMB of the Greenland Ice Sheet between 1980 and 2012 is 351 Gt yr^{-1} and the standard deviation is 98 Gt yr^{-1}. However, the spread among the 8 RCM and downscaled reanalyses is considerably smaller; these solutions lead to an average Greenland Ice Sheet SMB of 361 Gt yr^{-1} with a standard deviation of 40 Gt yr^{-1} over the same period. By comparison, the global reanalysis and process model lead to ice-sheet-wide estimates of SMB that are considerably larger (504 Gt yr^{-1}) and smaller (125 Gt yr^{-1}) than this range, respectively. Model resolution is an important factor when estimating SMB and its components, as respective contributions where only the spatial resolution differed yield regional differences. The underlying model domains were also identified as a source of discrepancy in the case of the Greenland Ice Sheet, as some products would allocate the ablation area outside the given mask.

Individual estimates of ice sheet mass balance

To standardize our comparison and aggregation of the 26 individual satellite estimates of Greenland Ice Sheet mass balance, we applied a common approach to derive rates of mass change from cumulative mass trends[41]. Rates of mass change were computed over 36-month intervals centred on regularly spaced (monthly) epochs within each cumulative mass trend time series, oversampling the individual time series where necessary. At each epoch, rates of mass change were estimated by fitting a linear trend to data within the surrounding 36-month time window using a weighted least-squares approach, with each point weighted by its measurement error. The associated mass trend uncertainties were estimated as the root sum square of the regression error and the measurement error. Time series were truncated by half the moving-average window period at the start and end of their period. The emerging rates of mass change were then averaged over calendar years to reduce the impact of seasonal cycles.

Gravimetry. We include 14 estimates of Greenland Ice Sheet ice sheet mass balance determined from GRACE satellite gravimetry that together span the period 2003– 2016 (Extended Data Fig. 1). Ten of the gravimetry solutions were computed using spherical harmonic solutions to the global gravity field and four were computed using spatially defined mass concentration units (Supplementary Table 1). An unrestricted range of alternative GIA corrections were used in the formation of the gravimetry mass balance solutions based on commonly adopted model solutions and their variants[34,51–57] (Supplementary Table 1). All of the gravimetry mass balance solutions included in this study use the same degree-1 coefficients to account for geocentre motion[58] and, although an alternative set is now available[96], the estimated improvement in certainty is small in comparison with their magnitude and spread. There was some variation in the sampling of the individual gravimetry datasets, and their collective effective (weighted mean) temporal resolution is 0.08 yr. Overall, there is good agreement between rates of Greenland Ice Sheet mass change derived from satellite gravimetry (Extended Data Fig. 5); all solutions show the ice sheet to be in a state of negative mass balance throughout their survey periods, with mass loss peaking in 2011 and reducing thereafter. During the period 2005–2015, annual rates of mass change determined from satellite gravimetry differ by 104 Gt yr^{-1} on average, and their average standard deviation is 31 Gt yr^{-1} (Extended Data Table 3).

Altimetry. We include nine estimates of Greenland Ice Sheet mass balance determined from satellite altimetry that together span the period 2004–2018 (Extended Data Fig. 1). Three of the solutions are derived from radar altimetry, four from laser altimetry and two use a combination of both (Supplementary Table 1). The altimetry mass trends are also computed using a range of approaches, including crossovers, planar fits and repeat track analyses. The laser altimetry mass trends are computed from ICESat-1 data as constant rates of mass change over their respective survey periods, whereas the radar altimetry mass trends are computed from EnviSat and/or CryoSat-2 data with a temporal resolution of between 1 and 72 months. In consequence, the altimetry solutions have an effective collective temporal resolution of 0.74 yr. Mass changes are computed after making corrections for alternative sources of surface elevation change, including glacial isostatic and elastic adjustment, and firn height changes (see Supplementary Table 1). Despite the range of input data and technical approaches, there is good overall agreement between rates of mass change determined from the various satellite altimetry solutions (Extended Data Fig. 5). All altimetry solutions show the Greenland Ice Sheet to be in a state of negative mass balance throughout their survey periods, with mass loss peaking in 2012 and reducing thereafter. During the period 2005–2015, annual rates of mass change determined from satellite altimetry differ by 121 Gt yr^{-1} on average, and their average standard deviation is 42 Gt yr^{-1} (Extended Data Table 3). The greatest variance lies among the 4 laser altimetry mass balance solutions, which range from −248 to −128 Gt yr^{-1} between 2004 and 2010; aside from methodological differences; possible explanations for this high spread include the relatively short period over which the mass trends are determined, the poor temporal resolution of these datasets and the rapid change in mass balance occurring during the period in question.

IOM. We include three estimates of Greenland Ice Sheet mass balance determined from the IOM that together span the period 1992–2015 (Extended Data Fig. 1). Although there are relatively few datasets in comparison with the gravimetry and altimetry solutions, the input–output data provide information on the partitioning of the mass change (surface processes and/or ice dynamics) cover a considerably longer period and are therefore an important record of changes in Greenland Ice Sheet mass during the 1990s. The IOM makes use of a wide range of satellite imagery (for example, refs. [6,40,97–102]) combined with measurements of ice thickness (for example, ref. [103]) for computing ice sheet discharge (output), and several alternative SMB model estimates of snow accumulation (input) and runoff (output) (see Supplementary Table 1). Two of the IOM datasets exhibit temporal variability across their survey periods, and ywo provide only constant rates of mass changes. Although these latter records are relatively short, they are an important marker with which variances among independent estimates can be evaluated. The collective effective (weighted mean) temporal resolution of the IOM data are 0.14 yr, although it should be noted that in earlier years the satellite ice discharge component of the data are relatively sparsely sampled in time (for example, ref. [104]).There is good overall agreement between rates of mass change determined from the input-output method solutions (Extended Data Fig. 5). During the period 2005–2015, annual rates of mass change determined from the four input–output datasets differ by up to 48 Gt yr^{-1} on average, and their average standard deviation is 23 Gt yr^{-1} (Extended Data Table 3). These differences are comparable to the estimated uncertainty of the individual techniques and are also small relative to the estimated mass balance over the period in question. In addition to showing that the Greenland Ice Sheet was in a state of negative mass balance since 2000, with mass loss peaking in 2012 and reducing thereafter, the IOM data show that the ice sheet was close to a state of balance before this period[33].

Aggregate estimate of ice sheet mass balance

To produce an aggregate estimate of Greenland Ice Sheet mass balance, we combine the 14 gravimetry, 9 altimetry and 3 IOM datasets to produce a single 26-yr record spanning the period 1992–2018. First, we combine the gravimetry, altimetry and the IOM data separately into three monthly time series by forming an error-weighted average of individual monthly rates of ice sheet mass change computed using the same technique (Extended Data Fig. 6). At each epoch, we estimate the uncertainty of these time-series as the root mean square of their component time-series errors. We then combine the mass balance time series derived from gravimetry, altimetry and the IOM to produce a single aggregate (reconciled) estimate, computed as the error-weighted mean of mass trends sampled at each epoch. We estimated the uncertainty of this reconciled rate of mass balance as either the root mean square departure of the constituent mass trends from their weighted-mean or the root mean square of their uncertainties, whichever is larger. Cumulative uncertainties are computed as the root sum square of annual errors, on the assumption that annual errors are not correlated over time. This assumption has been employed in numerous mass balance studies[1,17,33,41], and its effect is to reduce cumulative errors by a factor of 2.2 over the 5-yr periods we employ in this study (Table 1). If some sources of error are temporally correlated, the cumulative uncertainty may therefore be underestimated. In a recent study, for example, it is estimated that 30% of the annual mass balance error is systematic[105], and in this instance the cumulative error may be 37% larger. On the other hand, the estimated annual error on aggregate mass trends reported in this study (61 Gt yr^{-1}) are 70% larger than the spread of the independent estimates from which they are combined (36 Gt yr^{-1}) (Extended Data Table 3), which suggests the underlying errors may be overestimated by a similar degree. A more detailed analysis of the measurement and systematic errors is required to improve the cumulative error budget.

During the period 2004–2015, when all three satellite techniques were in operation, there is good agreement between changes in ice sheet mass balance on a variety of timescales (Extended Data Fig. 6). In Greenland, there are large annual cycles in mass superimposed on equally prominent interannual fluctuations as well as variations of intermediate (~5 yr) duration. These signals are consistent with fluctuations in SMB that have been identified in meteorological records[1,59], and are present within the time series of mass balance emerging from all three satellite techniques, to varying degrees, according to their effective temporal resolution. For example, correlated seasonal cycles are apparent in the gravimetry and IOM mass balance time series, because their effective temporal resolutions are sufficiently short (0.08 and 0.14 yr, respectively) to resolve such changes. However, at 0.74 yr, the effective temporal resolution of the altimetry mass balance time series is too coarse to detect cycles on sub-annual timescales. Nevertheless, when the aggregated mass balance data emerging from all three experiment groups are degraded to a common temporal resolution of 36 months, the time series are well correlated ($0.63 < r^2 < 0.80$) and, over longer periods, all techniques identify the marked increases in Greenland

Ice Sheet mass loss peaking in 2012. During the period 2005–2015, annual rates of mass change determined from all three techniques differ by up 162 Gt yr^{-1} on average, and their average standard deviation is 41 Gt yr^{-1}—a value that is small when compared with their estimated uncertainty (18 Gt yr^{-1}) (Extended Data Table 3).

Data availability

The aggregated Greenland Ice Sheet mass balance data and estimated errors generated in this study are freely available at http://imbie.org and at the NERC Polar Data Centre, https://doi.org/10.5285/8D5FF221-A470-4CC1-B7C4-CBDF383554FC.

Code availability

The code used to compute and aggregate rates of ice sheet mass change and their estimated errors are freely available at https://github.com/IMBIE.

51. Peltier, W. R., Argus, D. F. & Drummond, R. Space geodesy constrains ice age terminal deglaciation: the global ICE-6G_C (VM5a) model. *J. Geophys. Res. Solid Earth* **120**, 450–487 (2015).
52. Paulson, A., Zhong, S. & Wahr, J. Inference of mantle viscosity from GRACE and relative sea level data. *Geophys. J. Int*. **171**, 497–508 (2007).
53. Peltier, W. R. Global glacial isostasy and the surface of the Ice-Age Earth: the ICE-5G (VM2) model and GRACE. *Annu. Rev. Earth Planet. Sci*. **32**, 111–149 (2004).
54. Simpson, M. J. R., Milne, G. A., Huybrechts, P. & Long, A. J. Calibrating a glaciological model of the Greenland ice sheet from the Last Glacial Maximum to present-day using field observations of relative sea level and ice extent. *Quat. Sci. Rev*. **28**, 1631–1657 (2009).
55. A, G., Wahr, J. & Zhong, S. Computations of the viscoelastic response of a 3-D compressible Earth to surface loading: an application to glacial isostatic adjustment in Antarctica and Canada. *Geophys. J. Int*. **192**, 557–572 (2013).
56. Schrama, E. J. O., Wouters, B. & Rietbroek, R. A mascon approach to assess ice sheet and glacier mass balances and their uncertainties from GRACE data. *J. Geophys. Res. Solid Earth* **119**, 6048–6066 (2014).
57. Klemann, V. & Martinec, Z. Contribution of glacial-isostatic adjustment to the geocenter motion. *Tectonophysics* **511**, 99–108 (2011).
58. Swenson, S., Chambers, D. & Wahr, J. Estimating geocenter variations from a combination of GRACE and ocean model output. *J. Geophys. Res. Solid Earth* **113**, B08410 (2008).
59. Wouters, B., Bamber, J. L., van den Broeke, M. R., Lenaerts, J. T. M. & Sasgen, I. Limits in detecting acceleration of ice sheet mass loss due to climate variability. *Nat. Geosci*. **6**, 613–616 (2013).
60. Bonin, J. & Chambers, D. Uncertainty estimates of a GRACE inversion modelling technique over Greenland using a simulation. *Geophys. J. Int*. **194**, 212–229 (2013).
61. Blazquez, A. et al. Exploring the uncertainty in GRACE estimates of the mass redistributions at the Earth surface: implications for the global water and sea level budgets. *Geophys. J. Int*. **215**, 415–430 (2018).
62. Forsberg, R., Sørensen, L. & Simonsen, S. Greenland and Antarctica Ice Sheet Mass Changes and Effects on Global Sea Level. *Surv. Geophys*. **38**, 89–104 (2017).
63. Groh, A. & Horwath, M. The method of tailored sensitivity kernels for GRACE mass change estimates. *Geophys. Res. Abstr*. **18**, 12065 (2016).
64. Harig, C. & Simons, F. J. Mapping Greenland's mass loss in space and time. *Proc. Natl Acad. Sci. USA* **109**, 19934–19937 (2012).
65. Luthcke, S. B. et al. Antarctica, Greenland and Gulf of Alaska land-ice evolution from an iterated GRACE global mascon solution. *J. Glaciol*. **59**, 613–631 (2013).
66. Andrews, S. B., Moore, P. & King, M. A. Mass change from GRACE: a simulated comparison of Level-1B analysis techniques. *Geophys. J. Int*. **200**, 503–518 (2015).
67. Save, H., Bettadpur, S. & Tapley, B. D. High-resolution CSR GRACE RL05 mascons. *J. Geophys. Res. Solid Earth* **121**, 7547–7569 (2016).
68. Seo, K.-W. et al. Surface mass balance contributions to acceleration of Antarctic ice mass loss during 2003–2013. *J. Geophys. Res. Solid Earth* **120**, 3617–3627 (2015).
69. Velicogna, I., Sutterley, T. C. & van den Broeke, M. R. Regional acceleration in ice mass loss from Greenland and Antarctica using GRACE time-variable gravity data. *Geophys. Res. Lett*. **41**, 8130–8137 (2014).
70. Vishwakarma, B. D., Horwath, M., Devaraju, B., Groh, A. & Sneeuw, N. A data-driven approach for repairing the hydrological catchment signal damage due to filtering of GRACE products. *Wat. Resour. Res*. **53**, 9824–9844 (2017).
71. Wiese, D. N., Landerer, F. W. & Watkins, M. M. Quantifying and reducing leakage errors in the JPL RL05M GRACE mascon solution. *Wat. Resour. Res*. **52**, 7490–7502 (2016).
72. Ivins, E. R. & James, T. S. Antarctic glacial isostatic adjustment: a new assessment. *Antarct. Sci*. **17**, 541–553 (2005).
73. Ivins, E. R. et al. Antarctic contribution to sea level rise observed by GRACE with improved GIA correction. *J. Geophys. Res. Solid Earth* **118**, 3126–3141 (2013).
74. Rodell, M. et al. The Global Land Data Assimilation System. *Bull. Am. Meteorol. Soc*. **85**, 381–394 (2004).
75. Döll, P., Kaspar, F. & Lehner, B. A global hydrological model for deriving water availability indicators: model tuning and validation. *J. Hydrol*. **270**, 105–134 (2003).
76. Cheng, M., Tapley, B. D. & Ries, J. C. Deceleration in the Earth's oblateness. *J. Geophys. Res. Solid Earth* **118**, 740–747 (2013).
77. Balmaseda, M. A., Mogensen, K. & Weaver, A. T. Evaluation of the ECMWF ocean reanalysis system ORAS4. *Q. J. R. Meteorol. Soc*. **139**, 1132–1161 (2013).
78. Pujol, M.-I. et al. DUACS DT2014: the new multi-mission altimeter data set reprocessed over 20 years. *Ocean Sci*. **12**, 1067–1090 (2016).
79. Menemenlis, D. et al. ECCO2: High resolution global ocean and sea ice data synthesis. In *AGU Fall Meeting Abstracts 2008* OS31C-1292 (AGU, 2008).
80. Dobslaw, H. et al. Simulating high-frequency atmosphere-ocean mass variability for dealiasing of satellite gravity observations: AOD1B RL05. *J. Geophys. Res. Oceans* **118**, 3704–3711 (2013).
81. Carrère, L. & Lyard, F. Modeling the barotropic response of the global ocean to atmospheric wind and pressure forcing – comparisons with observations. *Geophys. Res. Lett*. **30**, 1275 (2003).
82. Csatho, B. M. et al. Laser altimetry reveals complex pattern of Greenland Ice Sheet dynamics. *Proc. Natl Acad. Sci. USA* **111**, 18478–18483 (2014).
83. Nilsson, J., Gardner, A., Sandberg Sørensen, L. & Forsberg, R. Improved retrieval of land ice topography from CryoSat-2 data and its impact for volume-change estimation of the Greenland Ice Sheet. *Cryosphere* **10**, 2953–2969 (2016).
84. Gourmelen, N. et al. CryoSat-2 swath interferometric altimetry for mapping ice elevation and elevation change. *Adv. Space Res*. **62**, 1226–1242 (2018).
85. Gunter, B. C. et al. Empirical estimation of present-day Antarctic glacial isostatic adjustment and ice mass change. *Cryosphere* **8**, 743–760 (2014).
86. Helm, V., Humbert, A. & Miller, H. Elevation and elevation change of Greenland and Antarctica derived from CryoSat-2. *Cryosphere* **8**, 1539–1559 (2014).
87. Kjeldsen, K. K. et al. Improved ice loss estimate of the northwestern Greenland ice sheet. *J. Geophys. Res. Solid Earth* **118**, 698–708 (2013).
88. Felikson, D. et al. Comparison of elevation change detection methods from ICESat altimetry over the Greenland Ice Sheet. *IEEE Trans. Geosci. Remote Sens*. **55**, 5494–5505 (2017).
89. Andersen, M. L. et al. Basin-scale partitioning of Greenland ice sheet mass balance components (2007–2011). *Earth Planet. Sci. Lett*. **409**, 89–95 (2015).
90. Colgan, W. et al. Greenland ice sheet mass balance assessed by PROMICE (1995–2015). *Geol. Surv. Denmark Greenl. Bull*. **43**, e2019430201 (2019).
91. van Wessem, J. M. et al. Updated cloud physics in a regional atmospheric climate model improves the modelled surface energy balance of Antarctica. *Cryosphere* **8**, 125–135 (2014).
92. Fettweis, X. et al. Estimating the Greenland ice sheet surface mass balance contribution to future sea level rise using the regional atmospheric climate model MAR. *Cryosphere* **7**, 469–489 (2013).
93. Wahr, J., Wingham, D. & Bentley, C. A method of combining ICESat and GRACE satellite data to constrain Antarctic mass balance. *J. Geophys. Res. Solid Earth* **105**, 16279–16294 (2000).
94. Lambeck, K., Rouby, H., Purcell, A., Sun, Y. & Sambridge, M. Closing the sea level budget at the Last Glacial Maximum. *Proc. Natl Acad. Sci. USA* **111**, 15861–15862 (2014).
95. Caron, L., Métivier, L., Greff-Lefftz, M., Fleitout, L. & Rouby, H. Inverting Glacial Isostatic Adjustment signal using Bayesian framework and two linearly relaxing rheologies. *Geophys. J. Int*. **209**, 1126–1147 (2017).
96. Sun, Y., Riva, R. & Ditmar, P. Optimizing estimates of annual variations and trends in geocenter motion and J2 from a combination of GRACE data and geophysical models. *J. Geophys. Res. Solid Earth* **121**, 8352–8370 (2016).
97. Nagler, T., Rott, H., Hetzenecker, M., Wuite, J. & Potin, P. The Sentinel-1 Mission: New Opportunities for Ice Sheet Observations. *Remote Sens*. **7**, 9371–9389 (2015).
98. Mouginot, J., Rignot, E., Scheuchl, B. & Millan, R. Comprehensive annual ice sheet velocity mapping using Landsat-8, Sentinel-1, and RADARSAT-2 data. *Remote Sens*. **9**, 364 (2017).
99. Joughin, I., Smith, B. E. & Howat, I. Greenland Ice Mapping Project: ice flow velocity variation at sub-monthly to decadal timescales. *Cryosphere* **12**, 2211–2227 (2018).
100. Lemos, A. et al. Ice velocity of Jakobshavn Isbræ, Petermann Glacier, Nioghalvfjerdsfjorden, and Zachariæ Isstrøm, 2015–2017, from Sentinel 1-a/b SAR imagery. *Cryosphere* **12**, 2087–2097 (2018).
101. Joughin, I. et al. Continued evolution of Jakobshavn Isbrae following its rapid speedup. *J. Geophys. Res. Earth Surf*. **113**, F04006 (2008).
102. Joughin, I., Abdalati, W. & Fahnestock, M. Large fluctuations in speed on Greenland's Jakobshavn Isbræ glacier. *Nature* **432**, 608–610 (2004).
103. Gogineni, S. et al. Coherent radar ice thickness measurements over the Greenland ice sheet. *J. Geophys. Res. D Atmospheres* **106**, 33761–33772 (2001).
104. Rignot, E. et al. Recent Antarctic ice mass loss from radar interferometry and regional climate modelling. *Nat. Geosci*. **1**, 106–110 (2008).
105. Shepherd, A. et al. Trends in Antarctic Ice Sheet elevation and mass. *Geophys. Res. Lett*. **46**, 8174–8183 (2019).
106. Martinec, Z. & Hagedoorn, J. The rotational feedback on linear-momentum balance in glacial isostatic adjustment. *Geophys. J. Int*. **199**, 1823–1846 (2014).
107. Fretwell, P. et al. Bedmap2: improved ice bed, surface and thickness datasets for Antarctica. *Cryosphere* **7**, 375–393 (2013).
108. Rignot, E., Mouginot, J. & Scheuchl, B. Ice flow of the Antarctic Ice Sheet. *Science* **333**, 1427–1430 (2011).
109. Rignot, E., Mouginot, J. & Scheuchl, B. Antarctic grounding line mapping from differential satellite radar interferometry. *Geophys. Res. Lett*. **38**, L10504 (2011).
110. Langen, P. L., Fausto, R. S., Vandecrux, B., Mottram, R. H. & Box, J. E. Liquid water flow and retention on the Greenland Ice Sheet in the regional climate model HIRHAM5: local and large-scale impacts. *Front. Earth Sci*. **4**, 110 (2017).
111. Martinec, Z. Spectral–finite element approach to three-dimensional viscoelastic relaxation in a spherical earth. *Geophys. J. Int*. **142**, 117–141 (2000).
112. Fleming, K. & Lambeck, K. Constraints on the Greenland Ice Sheet since the Last Glacial Maximum from sea-level observations and glacial-rebound models. *Quat. Sci. Rev*. **23**, 1053–1077 (2004).

113. King, M. A., Whitehouse, P. L. & van der Wal, W. Incomplete separability of Antarctic plate rotation from glacial isostatic adjustment deformation within geodetic observations. *Geophys. J. Int*. **204**, 324–330 (2016).
114. Spada, G., Melini, D. & Colleoni, F. SELEN v2.9.12 (Computational Infrastructure for Geodynamics, 2018); https://geodynamics.org/cig/software/selen.
115. Noël, B. et al. Evaluation of the updated regional climate model RACMO2.3: summer snowfall impact on the Greenland Ice Sheet. *Cryosphere* **9**, 1831–1844 (2015).
116. Noël, B. et al. A daily, 1 km resolution data set of downscaled Greenland ice sheet surface mass balance (1958–2015). *Cryosphere* **10**, 2361–2377 (2016).
117. Gelaro, R. et al. The Modern-Era Retrospective Analysis for Research and Applications, version 2 (MERRA-2). *J. Clim*. **30**, 5419–5454 (2017).
118. Wilton, D. J. et al. High resolution (1 km) positive degree-day modelling of Greenland ice sheet surface mass balance, 1870–2012 using reanalysis data. *J. Glaciol*. **63**, 176–193 (2017).
119. Mernild, S. H., Liston, G. E., Hiemstra, C. A. & Christensen, J. H. Greenland Ice Sheet surface mass-balance modeling in a 131-yr perspective, 1950–2080. *J. Hydrometeorol*. **11**, 3–25 (2010).

Acknowledgements This work is an outcome of the IMBIE supported by the ESA Climate Change Initiative and the NASA Cryosphere Program. A.S. was additionally supported by a Royal Society Wolfson Research Merit Award and the UK Natural Environment Research Council Centre for Polar Observation and Modelling.

Author contributions A.S. and E.I. designed and led the study. E.R., B.S., M.v.d.B., I.V. and P.W. led the IOM, altimetry, SMB, gravimetry and GIA experiments, respectively. G.K., S.N., T.P. and T. Scambos provided additional supervision on glaciology, K.B., A.H., I.J., M.E.E. and T.W. provided additional supervision on satellite observations and N.S. provided additional supervision on GIA. G.M., M.E.P. and T. Slater performed the mass balance data collation and analysis. T. Slater performed the AR5 data analysis. P.W. and I.S. performed the GIA data analysis. M.v.W. and T. Slater performed the SMB data analysis. A.S., E.I., K.B., M.E., N.G., A.H., H.K., M.M., I.O., I.S., T. Slater, M.v.W. and P.W. wrote the manuscript. A.S. led the writing, E.I., K.B., M.E., and T. Slater led the drafting and editing, M.v.W. led the SMB text, P.W. and I.S. led the GIA text and N.G., A.H., H.K., M.M. and I.O. contributed elsewhere. A.S., K.B., H.K., G.M., M.E.P, I.S., S.B.S., T. Slater, P.W. and M.v.W. prepared the figures and tables, with particular focus on Fig. 1 (S.B.S), Fig. 3 (T. Slater), Fig. 4 (T. Slater), Extended Data Fig. 2 (K.B.), Extended Data Fig. 3 (P.W.), Extended Data Fig. 2 (M.v.W.), Extended Data Table 1 (P.W. and I.S.), Extended Data Table 2 (M.v.W.) and Supplementary Table 1 (H.K. and T. Slater). G.M. and M.E.P. led the production of all other figures and tables. All authors participated in the data interpretation and commented on the manuscript.

Competing interests The authors declare no competing interests.

Additional information

Supplementary information is available for this paper at https://doi.org/10.1038/s41586-019-1855-2.

Correspondence and requests for materials should be addressed to A.S.

Peer review information *Nature* thanks Christina Hulbe, Andreas Kääb and the other, anonymous, reviewer(s) for their contribution to the peer review of this work.

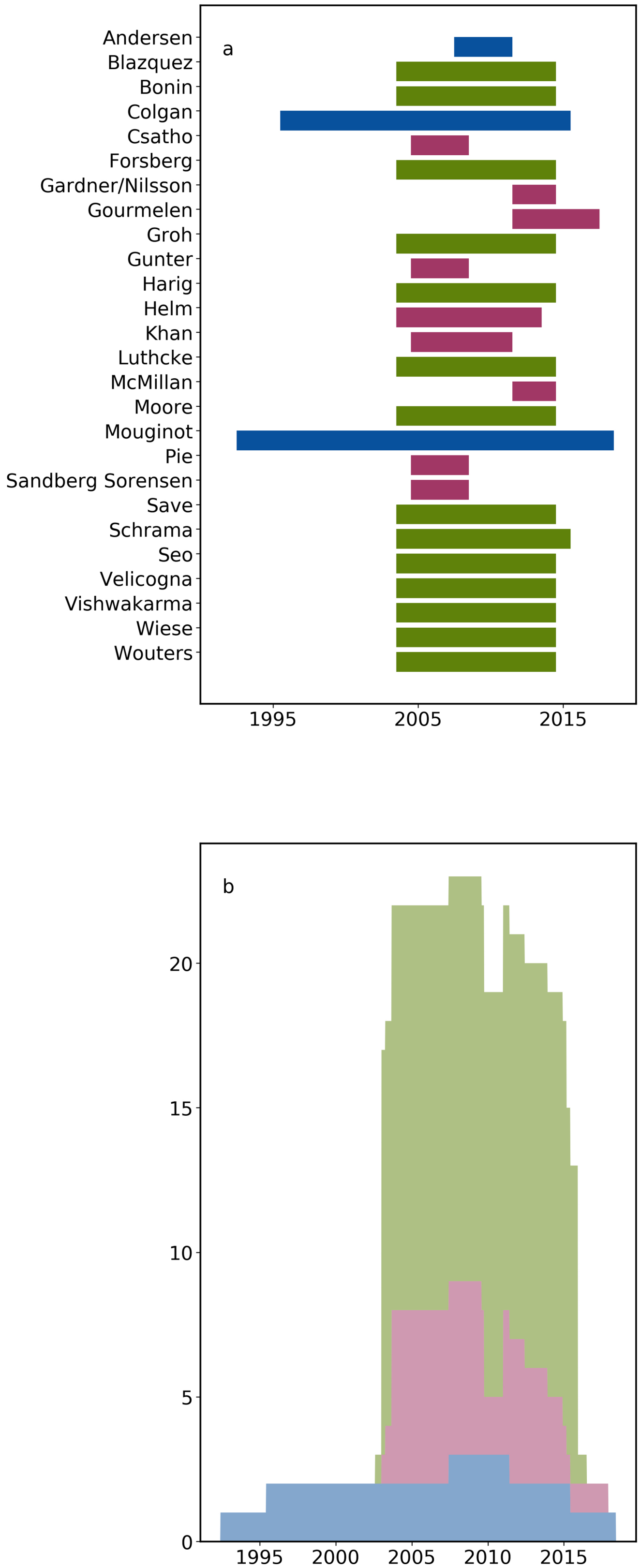

Extended Data Fig. 1 | Ice sheet mass balance datasets. a, Participant datasets used in this study and their main contributors. **b**, The number of data available in each calendar year. The interval 2003–2010 includes almost all datasets and is selected as the overlap period. Further details of the satellite observations used in this study are provided in Supplementary Table 1. Refs. [28,33,38,56,59–71,82–90].

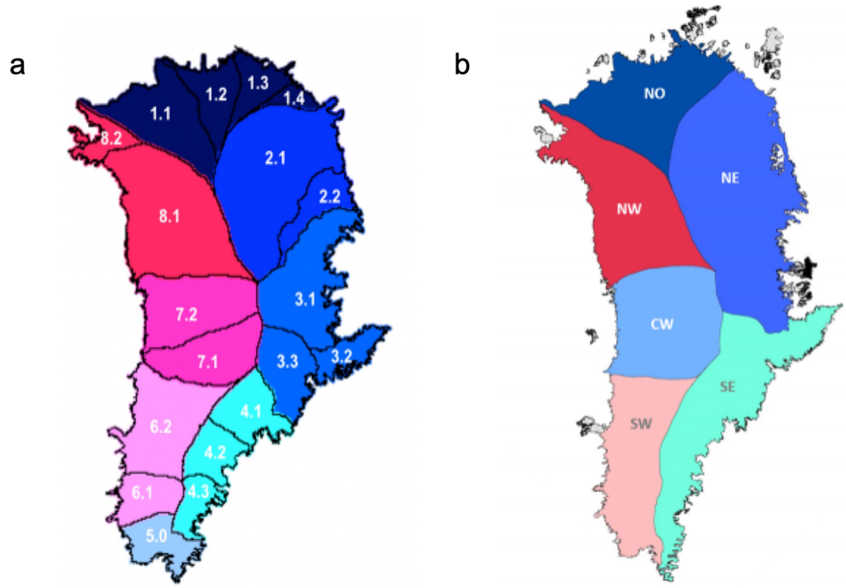

Extended Data Fig. 2 | Greenland Ice Sheet drainage basins. a, **b**, Basin used in this study, according to the definitions of ref. [20] (**a**) and ref. [37] (**b**).

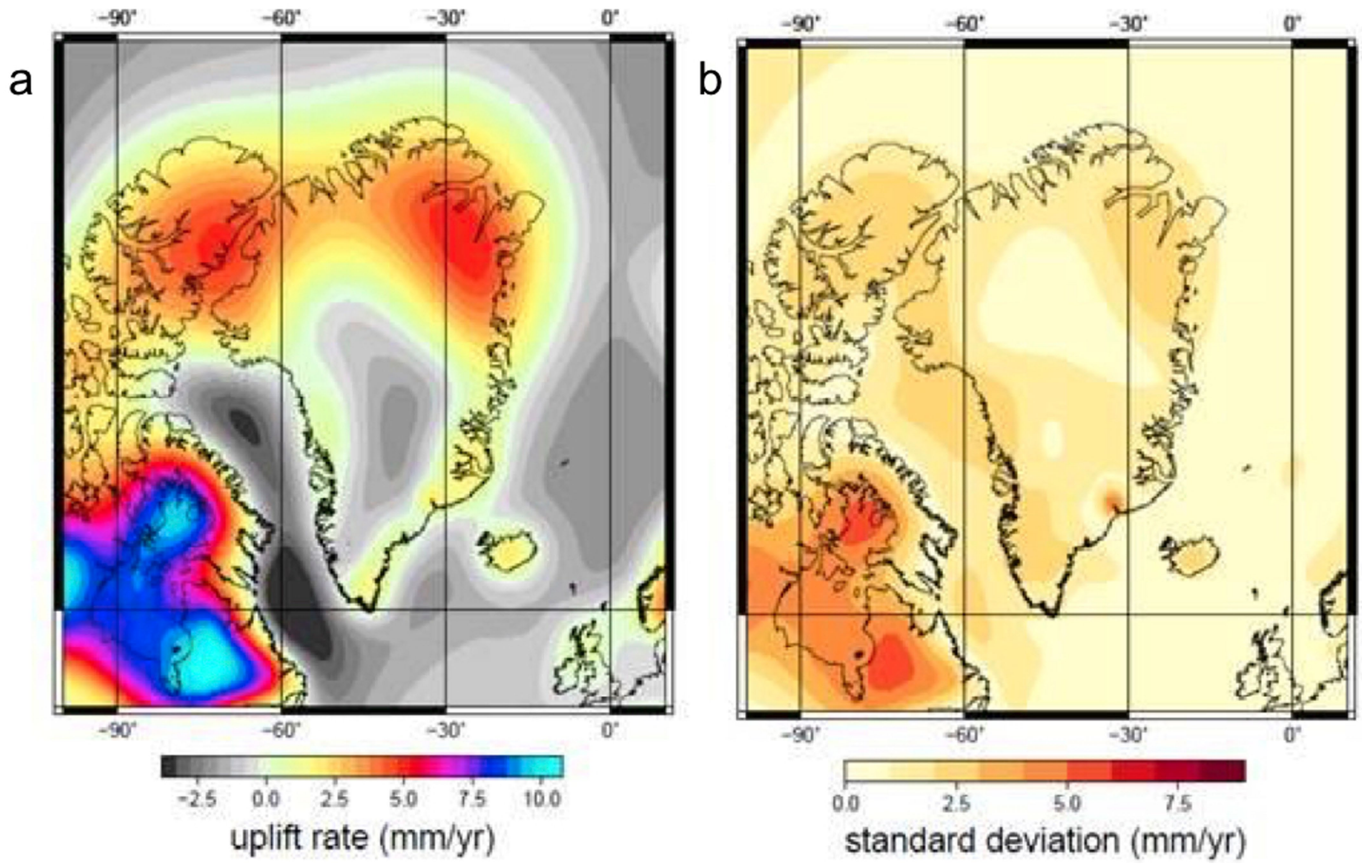

Extended Data Fig. 3 | Modelled glacial isostatic adjustment in Greenland. a, **b**, Bedrock uplift rates in Greenland averaged over the GIA model solutions used in this study (**a**) and their standard deviation (**b**). Further details of the GIA models used in this study are provided in Extended Data Table 1. High rates of uplift and subsidence associated with the former Laurentide Ice Sheet are apparent to the southwest of Greenland.

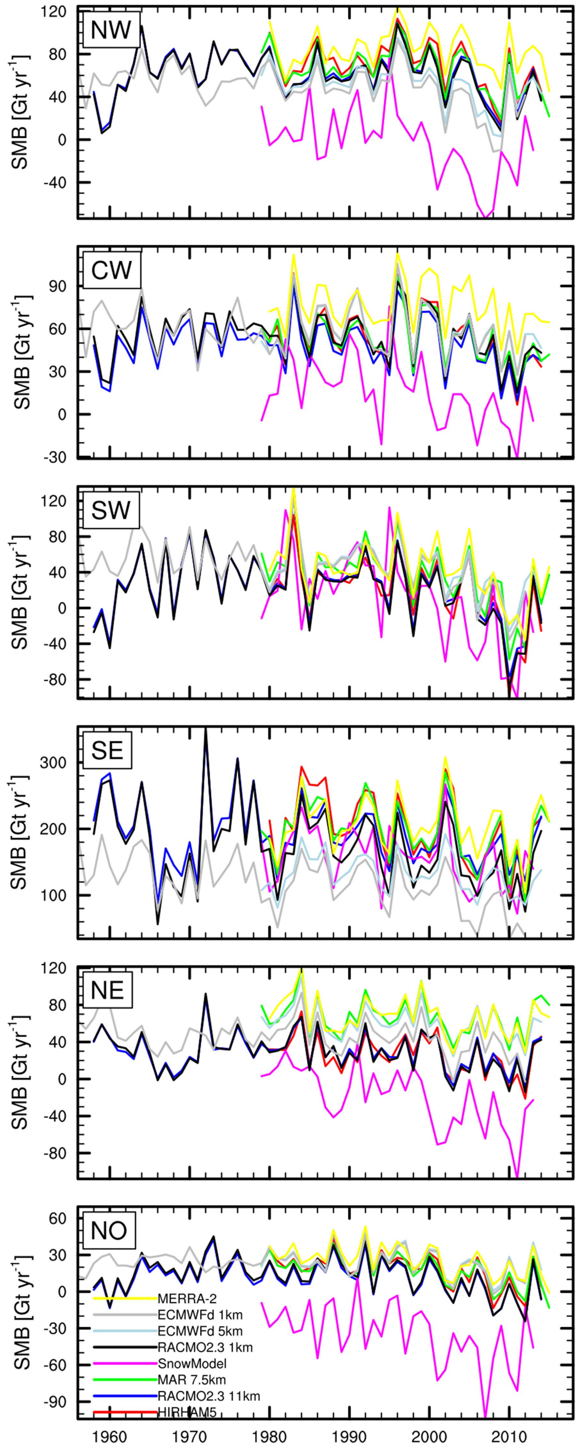

Extended Data Fig. 4 | SMB of the Greenland Ice Sheet. a–f, Time series of SMB in the NW, CW, SW, SE, NE and NO Greenland Ice Sheet drainage basins (Extended Data Fig. 2)[108,109]. Solid lines are annual averages of the monthly data (dashed lines). Further details of the SMB models used in this study are provided in Extended Data Table 2.

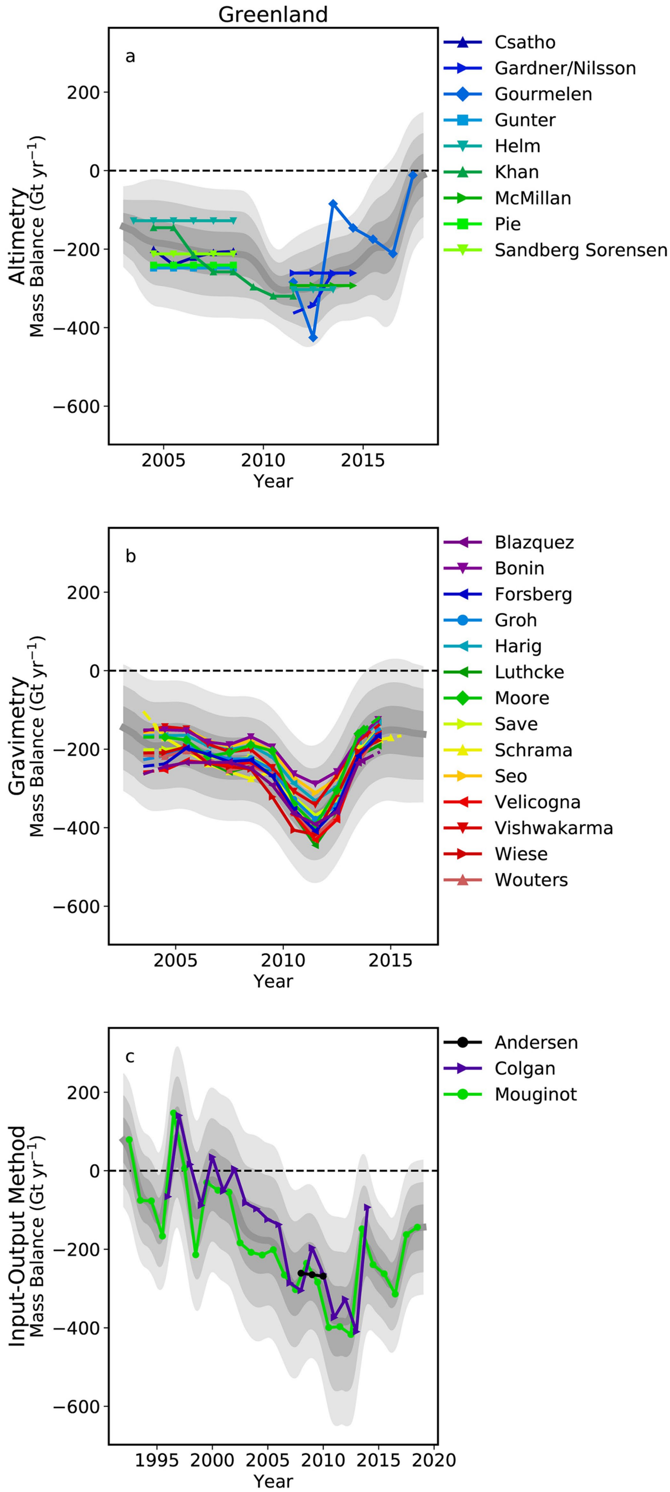

Extended Data Fig. 5 | Greenland Ice Sheet mass balance intracomparison. **a**–**c**, Individual rates of Greenland Ice Sheet mass balance used in this study as determined from satellite altimetry (**a**), gravimetry (**b**) and the input–output method (**c**). The grey shading shows the estimated 1σ (dark), 2σ (mid-) and 3σ (light) uncertainty relative to the ensemble average. Refs. [28,33,38,56,59–71,82–90].

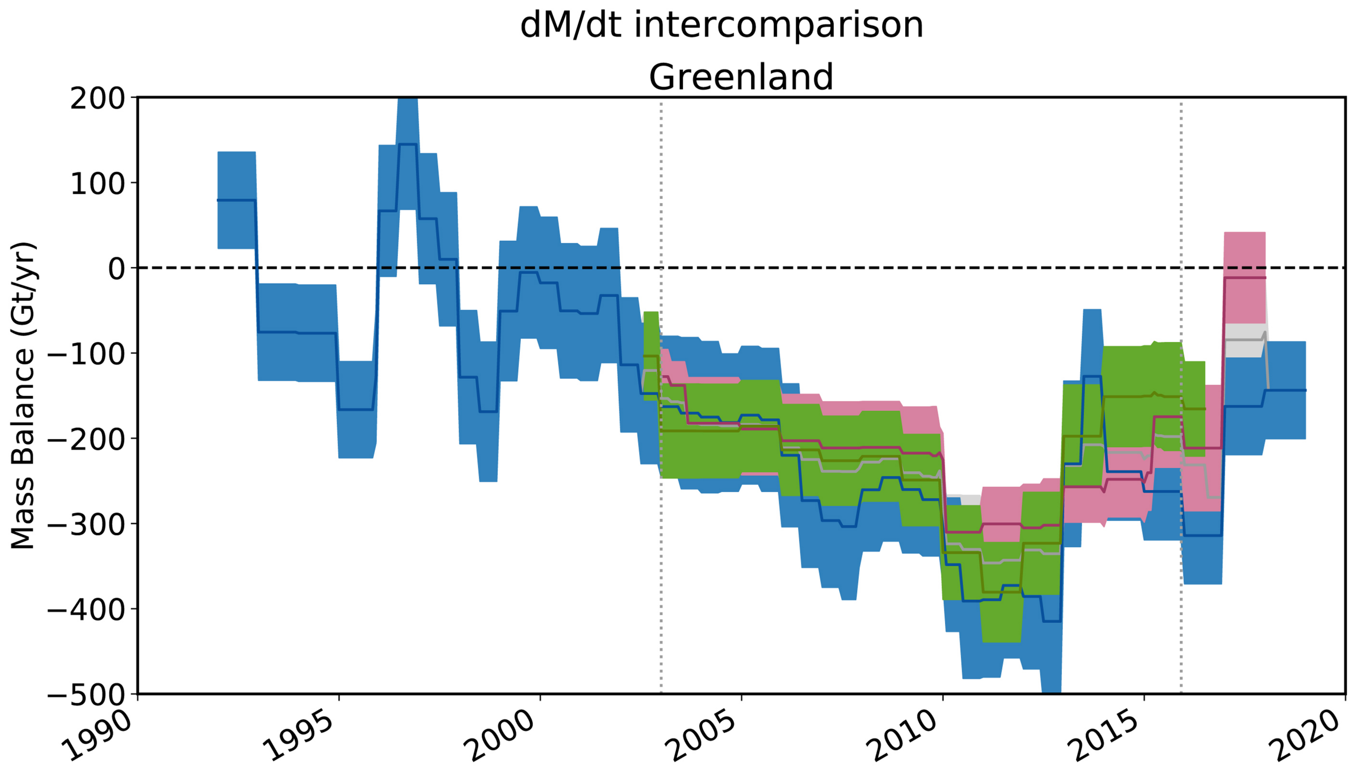

Extended Data Fig. 6 | Greenland Ice Sheet mass balance intercomparison. Rate of Greenland Ice Sheet mass balance as derived from the three techniques: satellite radar and laser altimetry (red), input–output method (blue) and gravimetry (green). Their arithmetic mean is shown in grey. The estimated uncertainty is also shown (shaded envelopes) and is computed as the root mean square of the component time-series errors.

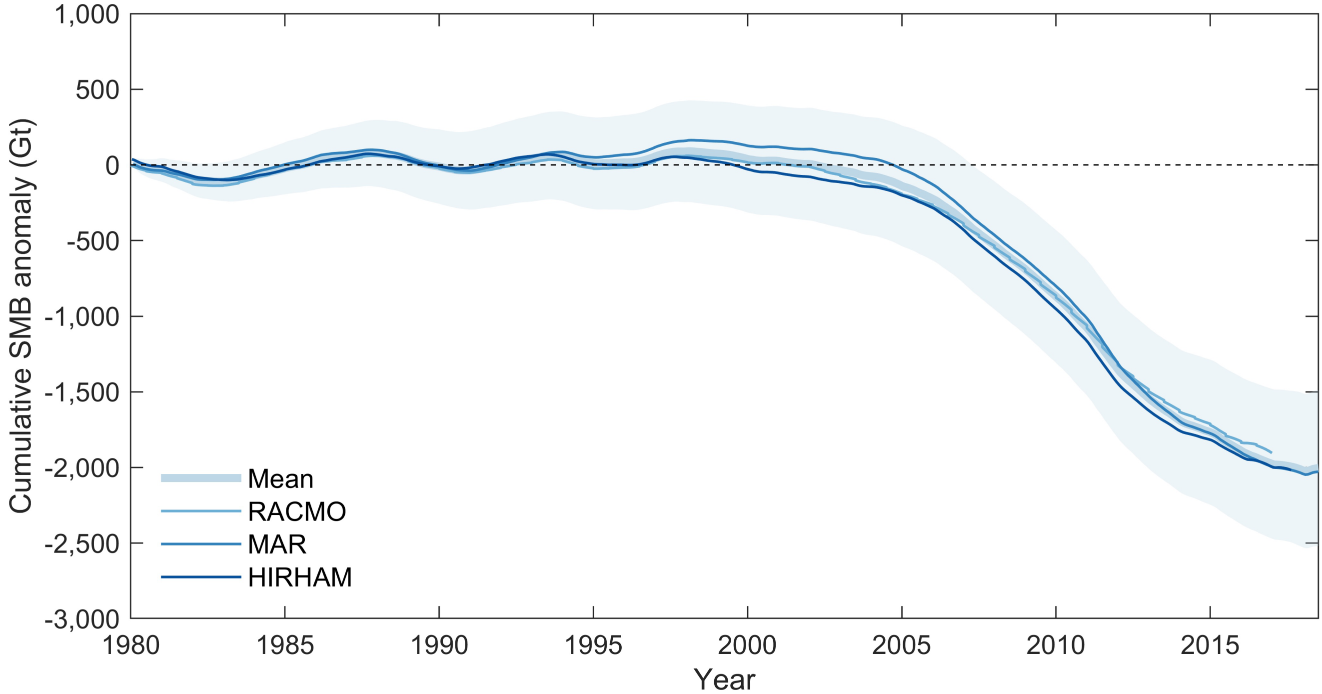

Extended Data Fig. 7 | Cumulative Greenland Ice Sheet SMB. The cumulative surface mass change determined from an average (mean) of the RACMO2.3p2[46], MARv3.6[21] and HIRHAM[9] regional climate models relative to their 1980–1990 means (see Methods). The estimated uncertainty of the mean change is also shown (shaded area), computed as the average of the uncertainties from each of the three models. RACMO2.3p2 uncertainties are based on a comparison to in situ observations[33]. MARv3.6 uncertainties are evaluated from the variability due to forcing from climate reanalyses[21]. HIRHAM uncertainties are estimated on the basis of comparisons to in situ accumulation and ablation data[110]. Cumulative uncertainties are computed as the root sum square of annual errors, on the assumption that these errors are not correlated over time[17].

Extended Data Table 1 | Details of GIA models used in this study

Contributor	Model	Publication [a]	Earth model [b]	Ice model [b]	GIA model [c]	Constraint data [d]	GIA (Gt/yr)
A	A13	A et al., 2013	VM5a (1D) [e]	ICE-6G_C [f]	SH, C, RF, SG, OL	As for ICE-6G_C [f]	-9‡
Lecavalier	Huy3	Lecavalier et al., 2014	1D (120, 0.5, 2)	Huy3/ICE-5G	SH(256), IC, RF, SG, OL	RSL, ice extent, paleo thinning rates	-19‡
Sasgen	GGG1D.0	Khan et al., 2016 Martinec, 2000	VM-GPS [42]	modified GREEN1 [79]	SH(256)/FE(radial), IC, RF, SG, OL	GPS, RSL	+17†
Peltier	ICE-6G_D (VM5a)	Peltier et al., 2015	VM5a (1D) [e]	ICE-6G_D [g]	SH(512)	GPS, RSL, Earth rotation	-10‡
van der Wal	SL-dry-4mm/W12	King et al., 2016	3D, power-law rheology	Combination of W12 (Antarctica) and ICE-5G	FE, IC, xRF	GPS, RSL, seismic velocities (Earth model)	+21‡
Spada	SELEN 4	Spada et al., 2018	VM5a (3-layer average of 1D model) [e]	ICE-6G_C [f]	SELEN4: SH(128), IC, RF, SG, OL	As for ICE-6G_C [f]	-27‡

Refs. [34,42,51,55,111,113,114].

†Regional changes in mass associated with the GIA signal determined by the contributor.

‡Regional changes in mass associated with the GIA signal calculated as an indicative rate using spherical-harmonic degrees 3 to 90 and a common treatment of degree 2 (ref. [106]).

[a]Main reference publication(s).

[b]Model from main publication unless otherwise stated. Comma-separated values refer to properties of a radially varying (1D, one-dimensional) Earth model: the first value is lithosphere thickness (km), other values reflect mantle viscosity (x 10^{21} Pa s) for specific layers; see relevant publication.

[c]GIA model details: SH = spherical harmonic (maximum degree indicated), FE = finite element, C = compressible, IC = incompressible, RF = rotational feedback, SG = self-gravitation, OL = ocean loading, 'x' = feature not included.

[d]RSL = relative sea-level data; GPS rates corrected for elastic response to contemporary ice mass change.

[e]Earth model taken from ref. [51].

[f]Ice model taken from ref. [51].

[g]Different to ICE-6G_C in Antarctica, owing to the use of Bedmap2[107] topography.

Extended Data Table 2 | Details of the SMB models used in this study

Contributor	Model	Publication [a]	Class [b]	Area (10^6 km^2)	Grid	SMB [c] (Gt/yr)	Precipitation [c] (Gt/yr)	Runoff [c] (Gt/yr)
Noël	RACMO2.3	Noël et al., 2015	RCM	1.73	11 km	350	721	311
Noël	RACMO2.3p2	Noël et al., 2018	RCM	1.73	11 km	432	727	258
Langen	HIRHAM5	Lucas-Picher et al., 2012	RCM	1.71	5.5 km	385	794	351
Fettweis	MARv3.6	Fettweis et al., 2017	RCM	1.69	7.5 km	381	706	308
Noël	RACMO2.3d	Noël et al., 2016	RCM-d	1.69	1 km	314	755	397
Noël	RACMO2.3p2d	Noël et al., 2018	RCM-d	1.69	1 km	338	703	331
Cullather	MERRA-2	Gelaro et al., 2017	GA-n	1.73	0.5 °	504	818	277
Hanna	ECMWF	Hanna et al., 2012	GA-d	1.65	5 km	370	532	186
Wilton	ECMWFd	Wilton et al., 2017	GA-d	1.71	1 km	314	603	246
Mernild	Snow Model	Mernild et al., 2010	PM	1.64	5 km	125	655	418

Refs. [9,13,21,46,115–119].

[a]Main reference publication; additional references are provided in Supplementary Table 1.

[b]SMB model class; regional climate model (RCM), global numerical analysis (GA), process model (PM). Native resolution (n) and downscaled (d) models are also identified.

[c]Averages over the period 1980–2012 for the Greenland Ice Sheet excluding peripheral ice caps and using the drainage basins from ref. [37].

Extended Data Table 3 | Rate of Greenland Ice Sheet mass change for 2005–2015

Technique	Mass balance (Gt/yr)	s.d.(Gt/yr)	range (Gt/yr)
Altimetry*	-244 ± 15	43	122
Gravimetry	-248 ± 18	31	104
Input-Output Method	-281 ± 25	23	48
All	-255 ± 20	41	163

Estimates of ice-sheet mass balance from satellite altimetry, gravimetry the input–output method and from all three groups during the period 2005–2015. The average s.d. and ranges of individual estimates within each group during the same period are also shown. *No altimetry data in 2010.